A Study on New Synthesis of CdS and CdSe Nanoparticles and Their Organic/Inorganic Nanocomposites

CdS와 CdSe 나노입자의 새로운 합성과 그들의 유기/무기 나노복합체에 관한 연구

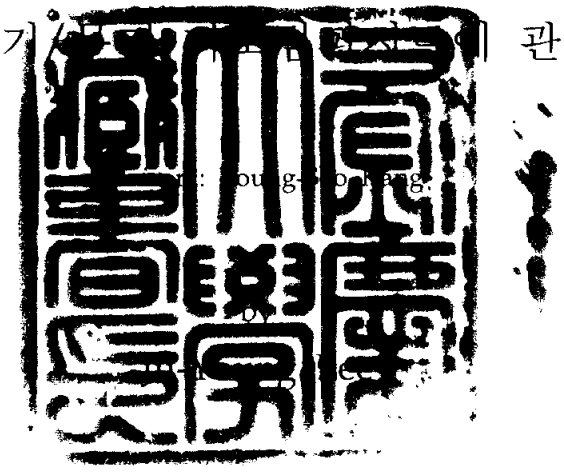

A thesis submitted in partial fulfillment of the requirements.

for the degree of

Master of Science

in the Departement of Chemistry, Graduate School,

Pukyong National University

February 2004

A Study on New Synthesis of CdS and CdSe Nanoparticles and Their Organic/Inorganic Nanocomposites

A Dissertation

by

Ju-Young Lee

Approved as to style and content by :

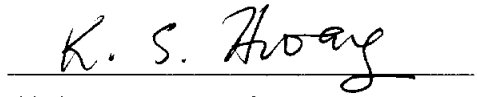

Chair man : Kum Sho Hwang

Member : Don Kim

Member : Young Soo Kang

December 2003

Contents

Abstract ····· 1

1. Introduction ····· 2

2. Experimental ····· 5

2-1. Materials ····· 5

2-1-1. Preparation of CdS and CdSe nanoparticles ····· 5

2-1-2. Preparation of PVA/CdS and PVA/CdSe nanocomposites ··· 6

2-1-3. Preparation of LDPE/CdS and LDPE/CdSe nanocomposites ··· 6

2-1-4. Surfactants ····· 7

2-2. Methods ····· 8

2-2-1. Background ····· 8

2-2-2. Experimental technique ····· 21

3. Result and Discussion ····· 23

3-1. Characterization of CdS and CdSe nanoparticles ····· 23

3-1-1. X-ray powder diffraction (XRD) study ····· 23

3-1-2. Transmission electron microscopy (TEM) ····· 24

3-1-3. High Resolution Transmission electron microscopy (HRTEM) ···· 26

3-1-4. Electron diffraction (ED) ····· 26

3-1-5. Energy dispersive X-ray (EDX) spectrometer ····· 28
3-1-6. UV-vis study ····· 31
3-1-7. Photoluminescence (PL) study ····· 32
3-1-8. Photoluminescence images ····· 34

3-2. Coverage calculation of CdS surrounding with organic surfactant ·· 36
3-2-1. Thermogravimetric analysis (TGA) ····· 36
3-2-2. Surface pressure-area isotherm ····· 37
3-2-3. Coverage calculation ····· 40
3-2-4. Transmission electron microscopy (TEM) ····· 41
3-2-5. Atomic force microscopy (AFM) ····· 42

3-3. Characterization of PVA/CdS and CdSe nanocomposites ····· 46
3-3-1. UV-vis absorption spectra ····· 46
3-3-2. UV-vis transmission spectra ····· 48
3-3-3. Photoluminescence (PL) study ····· 48
3-3-4. Optical images ····· 51

3-4. Characterization of LDPE/CdS and CdSe nanocomposites ····· 52
3-4-1. UV-vis absorption spectra ····· 52
3-4-2. UV-vis transmission spectra ····· 54
3-4-3. Photoluminescence (PL) study ····· 54
3-4-4. Optical images ····· 54
3-4-5. Scanning electron microscopy (SEM) ····· 55

4. Conclusion 56

5. References 57

6. Korean abstract 62

List of Figures

Figure 1 Molecular structures of (a) low density polyethylene (LDPE) and (b) polyvinyl acetate (PVA).

Figure 2 Electronic energy levels depending on the number of bound atoms. By binding more and more atoms together, the discrete energy levels of the atomic orbitals merge into energy bands (here shown for a semiconducting material).[40]

Figure 3 Schematic drawings of expanded and compressed monolayers on a water surface.

Figure 4 Schematic drawings of deposition of the first monolayer onto a hydrophobic substrate.

Figure 5 Pressure-area isotherm of a fatty acid on the pure water surface.

Figure 6 Typical experimental set-up for PL measurements.

Figure 7 Schematic drawings of Langmuir-Blodgett deposition of oleate/CdS nanoparticle complex monolayer at the air/water interface.

Figure 8 X-ray powder diffraction (XRD) patterns of CdS and CdSe nanoparticles. These nanoparticles are capped with oleate as a capping surfactant.

Figure 9 Transmission electron microscopy (TEM) images of (a) CdS and (b) CdSe nanoparticles.

Figure 10 High resolution transmission electron microscopy (HRTEM) lattice images of (a) and (b) of CdS and (c) and (d) of CdSe nanoparticles.

Figure 11 Electron diffraction (ED) patterns of (a) CdS and (b) CdSe nanoparticles.

Figure 12 Energy dispersive X-ray spectra of (a) CdS and (b) CdSe nanoparticles.

Figure 13 UV-vis spectra of CdS and CdSe nanoparticles.

Figure 14 Photoluminescence spectra of CdS and CdSe nanoparticles.

Figure 15 Photoluminescence images of CdS and CdSe solutions according to irradiation of UV lamp (solvent : iso-octane).

Figure 16 TGA graph of CdS nanoparticles containing oleate.

Figure 17 Surface pressure-area isotherm of CdS nanoparticles containing oleate in the subphase of pure water at room temperature.

Figure 18 Surface pressure-area isotherm of stearic acid in the subphase of pure water at room temperature.

Figure 19 Schematic drawings of oleate/CdS nanoparticles for coverage calculation.

Figure 20 Transmission electron microscopy (TEM) image of Langmuir- Blodgett film of CdS nanoparticles prepared by Langmuir-Blodgett technique.

Figure 21 Top view on the surface image (a) and three-dimensional surface morphology (b) of Langmuir-Blodgett film of CdS nanoparticle deposited onto mica surface at 25 mN/m surface pressure with two layer obtained with AFM.

Figure 22 Top view on the surface image (a) and three-dimensional surface morphology (b) of Langmuir-Blodgett film of CdS nanoparticle deposited onto mica surface at 15 mN/m surface pressure by two layers obtained with AFM.

Figure 23 UV-vis absorption spectra of PVA/CdS and PVA/CdSe nanocomposites.

Figure 24 UV-vis transmission spectra of PVA/CdS and PVA/CdSe nanocomposites.

Figure 25 Photoluminescence spectra of (a) PVA/CdS, (b) PVA/CdSe nanocomposites according to concentration of CdS and CdSe nanoparticles, respectively.

Figure 26 Optical images of PVA/CdS and PVA/CdSe nanocomposite.

Figure 27 UV-vis absorption spectra of LDPE/CdS and LDPE/CdSe nanocomposites.

Figure 28 UV-vis transmission spectra of LDPE/CdS and LDPE/CdSe nanocomposites.

Figure 29 Photoluminescence spectra of LDPE/CdS and LDPE/CdSe nanocomposites.

Figure 30 Optical images of LDPE/CdS and LDPE/CdSe nanocomposites.

Figure 31 Scanning electron microscopy (SEM) image of the section of LDPE/CdS nanocomposite.

List of Tables

Table 1 Wavelength color according to wavelength range of 340 - 700 nm.

Table 2 UV-vis absorption wavelength (λ_{max}) of various polymer materials.

A Study on a New Synthesis of CdS and CdSe Nanoparticles and Their Organic/Inorganic Nanocomposites

Ju Young Lee

Department of Chemistry, Graduate School
Pukyong National University

Abstract

Nanoparticles of CdS and CdSe were synthesized by thermal treatment using autoclave method using sodium oleate as complexing surfactant. Sodium oleate has been used as effective stabilizers for the synthesis of CdS and CdSe nanoparticles by autoclave method. The materials such as CdS and CdSe inorganic nanoparticles have a photoluminescence (PL). PL of CdS and CdSe nanoparticles with particle size range of 2.6 - 13 nm showed λ_{max} at 512 nm and 600 nm, respectively, when excited at 365 nm. PL of the synthesized nanoparticles showed wavelength modification into visible region when excited at UV light. These nanoparticles doped into the PVA or LDPE resin resulted in the organic/inorganic nanocomposites (PVA or LDPE/CdS, CdSe). The longevity of films such as PVA, LDPE is reduced by a degradation of the double bonds of C=O and C=C in the polyolefin films by ultraviolet (UV) irradiation. As a result, the physical properties of the films are changed. This is suppressed by doping wavelength modifying nanoparticles into the films to absorb UV light which gives damage on films. The synthesized nanoparticles and nanocomposites were characterized by absorption, transmission, fluorescence, X-ray powder diffraction (XRD), optical images, transmission electron microscopy (TEM) and scanning electron microscopy (SEM).

1. Introduction

Colloidal nanoparticles have attracted broad attention from researchers in various disciplines.[1] Nanoparticles have their unique properties due to the quantum size effect and size-dependent characteristics.[2,3] Semiconductor nanoparticles have been applied to many different technological areas including biological labeling and diagnostics, light-emitting diodes, electroluminescent devices, photovoltaic devices, lasers and single-electron transistors.[4] Control of particle size and surface structure continues to be of interest in the investigation of semiconductor nanoparticles because of the high surface-to-volume ratio of nanoparticles, their peculiar structure and optical properties.[5-8] Many synthetic methods, which normally include arrested precipitation in homogeneous solution and synthesis in confined reaction vessels such as reverse micelles[9] and vesicles[10], have been developed for the chemical preparation of relatively monodisperse nanoparticles of various semiconductor materials. Specially, high-quality nanoparticles of CdS, a typical semiconductor material, have been synthesized via arrested precipitation from simple inorganic ions using polyphosphate[11] and low molecular weight thiols[12,13] as stabilizers, from dimethylcadmium in trioctyl phosphine (TOP) using trioctylphosphine oxide (TOPO) as a stabilizer,[14] and cadmium 2-ethylhexanoate in dimethyl sulfoxide (DMSO) using ethylhexanoate as a stabilizer.[15]

Synthetic methods empolying polymers and glasses produce size-polydisperse products.[16,17] Zeolites limit nanoparticles diameters to pore dimensions[18,19,20] and lithographic technology cannot reach the

necessary resolution,[18,21] to synthesize size-quantized II-VI materials, such as CdS or CdSe. Ion-sputtering technology produces crystalline GaSb quantum dots of 35 nm in diameter that are arranged in a regular hexagonal lattice but has not been used for CdS.[22] Reverse/irreverse micelle systems, with surfactants and copolymers give a well-controlled size distribution with the diameter smaller than that of the micelles.[23,24] Sol-gel methods with the aging of a highly concentrated solution of Cd^{2+} ion in combination with chelating agents at room temperature can produce a uniform-disperse product with a mean diameter of 43.9 - 249 nm.[25] Single-molecule precursors synthetic approaches offer high quality CdS or CdSe nanoparticles obtained by re-isolation and re-dispersion of the product to reach an average size and size distribution of 50 ± 8 Å.[26] A thermolysis method using trioctylphosphine sulfide (TOPS) can produce similar quality CdS nanoparticles by refluxing air-sensitive starting reagents with TOPO but the yield and size distribution data are not available.[27] The synthesis of colloidal inorganic nanocrystals especially with respect to the control of their shape, however, is under developing and still complicated. Although many synthetic techniques for such nanoparticles have been developed, nanoparticles are still obtained as aggregated state in organic or inorganic media. A new direction for synthetic methods and an understating of the mechanisms on how size and shape of the nanocrystals can be easily varied are key issues in nanochemistry.

In this paper, we demonstrate a new synthetic method for CdS and CdSe nanoparticles using sodium oleate as capping organic surfactant by thermal treatment. Sodium oleate has been used as specific stabilizer for the synthesis of CdS and CdSe nanoparitlces having

various properties such as dispersion ability. The Langmuir-Blodgett film of the synthesized CdS nanoparticle was prepared by Langmuir-Blodgett techniques. The Langmuir behavior of the complex monolayer at the air/water interface was studied with pressure-area isotherm. To achieve a stable nanocomposite Langmuir layer composed of surfactant and nanoparticles, it is necessary to study phase behavior of the monolayer complex at the air/water interface. The surface pressure can be increased by compressing the monolayer and increasing the surface concentration. In the compressed monolayer, the CdS nanoparticles attach to the surface of the monolayer surfactant at the air/water interface. According to the obtained data, we could calculate the coverage of CdS surrounding with organic surfactant. Also, we revealed the stability in the polymer resins such as polyvinyl acetate (PVA) and low density polyethylene (LDPE) for the preparation of functional nanocomposite. The characterization of the synthesized CdS and CdSe nanoparticles was carried out with XRD and UV-vis, photoluminescence (PL) spectroscopy. The size distribution of the synthesized CdS and CdSe nanoparticle in the complex and homogeneous dispersion was investigated with Transmission Electron Microscopy (TEM). The surface morphology of surfactant monolayer/CdS nanoparticle complex was studied with Atomic Force Microscopy (AFM).

2. Experimentals

2-1. Materials

2-1-1. Preparation of CdS and CdSe nanoparticles

Cadmium chloride hemipentahydrate ($CdCl_2 \cdot 5/2H_2O$, Aldrich), sodium oleate ($C_{17}H_{33}COONa$, Junsei) and sodium sulfide nonahydrate ($Na_2S \cdot 9H_2O$, 98^+%, Aldrich) were used in their commercial form. NaHSe powders were prepared by the reaction between selenium and sodium borohydride in water. Acetone and iso-octane were all of the highest quality commercially available. Distilled water was passed through a six-cartridge Barnstead Nanopure II purification train consisting of Macropure treatment.

The synthesis of CdS and CdSe nanoparticles was achieved by reaction of Na_2S and NaHSe in an aqueous solution. In case of CdS, cadmium chloride and sodium sulfide are employed as starting reagents that are dissolved in water. Sodium oleate is chosen as a surfactant to passivate the surface of CdS nanoparticles. All of the materials were the highest quality commercially available. In a typical procedure, a 80 ml of mixed solution containing 0.125 M sodium oleate and water was prepared and stirred for 20 min. Then, a 5.0 ml of 6.25×10^{-2} M $CdCl_2$ was added. The resulting solution was allowed to be stirred for 30 min and 6.25×10^{-2} M $Na_2S \cdot H_2O$ was added and followed by stirring for 2 hrs to form yellow solution. This solution was put into an autoclave of 100 ml capacity and maintained at 300 ℃ for 2 hrs and air-cooled to room temperature.

Precipitation occurs to form nanoparticles of CdS. Afterward, the precipitates were washed with acetone and filtered to remove the residues of impurities. The bright yellow product was dried at room temperature. CdSe nanoparticles were synthesized with the same method. The size of the nanoparticles prepared by this synthetic route is tunable by variation of the reaction time and control of the reaction temperature; in addition, the resulting sizes are suitable for spectroscopic testing of electron quantum confinement.

2-1-2. Preparation of PVA/CdS and PVA/CdSe nanocomposites

PVA resin having pellet shape was obtained by commercial form. A 16 g of PVA pellet was dissolved in 50 ml of acetone to make PVA solution. As the same method, a 1×10^{-3} g of CdS or CdSe nanoparticles was added in 1 ml of acetone. A 4.0 ml of PVA solution was mixed with 0.09 wt% of resulting CdS or CdSe dissolved in acetone and loaded into a round container. In accordance with the concentration, 0.87 and 2.62 wt% of CdS dissolved in acetone were added in PVA solution. The mixture was left for 24 hrs at room temperature. Finally, the transparent PVA nanocomposite films containing CdS or CdSe were obtained.

2-1-3. Preparation of LDPE/CdS and LDPE/CdSe nanocomposites

LDPE resin having pellet shape was obtained by commercial form. In case of LDPE, a 10 g of LDPE was added in 100 ml of toluene and then heated at 80 ℃ for 2 hrs. CdS or CdSe solutions of toluene was added in LDPE solution and then leaved at 40 ℃ until

to result in the LDPE/CdS or CdSe nanocomposites. The synthesized LDPE/CdS or LDPE/CdSe nanocomposites were prepared to film by press machine.

2-1-4. Surfactant and Polymer resins

In this work, surfactant and polymer resins such as polyvinyl acetate (PVA), low density polyethylene (LDPE) were used. The used surfactant was sodium oleate. Surfactant induced aggregation or crystallization of organic and inorganic materials have been studied to obtain information on crystal growth and electron transport processes occurring within limited distances between nuclei.[28-35] PVA and LDPE resins were utilized to make nanocomposites.

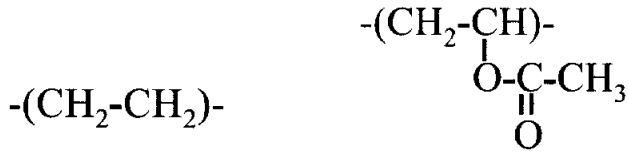

(a) (b)

Figure 1 Molecular structures of (a) low density polyethylene (LDPE) and (b) polyvinyl acetate (PVA).

2-2. Methods

2-2-1. Background

Nanoscale science and technology : In the last decade new directions of modern research, broadly defined as "nanoscale science and technology" have emerged.[36,37] These new trends involve the ability to fabricate, characterize, and manipulate artificial structures, whose features are controlled at the nanometer level. They embrace areas of research as diverse as engineering, physics, chemistry, materials science, and molecular biology. Research in this direction has been triggered by the recent availability of revolutionary instruments and approaches that allow the investigation of material properties with a resolution close to the atomic level. Strongly connected to such technological advances are the pioneering studies that have revealed new physical properties of matter at a level which is intermediate between atomic and molecular level and bulk. Materials science and technology is a field that is evolving at a very fast pace and is currently making the most significant contributions to nanoscale research. It is driven by the desire to fabricate materials with novel or improved properties. Such properties can be for instance strength, electrical and thermal conductivity, optical response, elasticity or wear-resistance. Research is also evolving towards materials that are designed to perform more complex and efficient tasks. Examples include materials with a higher rate of decomposition of pollutants, a selective and sensitive response toward a given biomolecule, an improved conversion of light into current or more efficient energy storage. For such and more complex tasks to be realized, novel

materials have to be based on several components whose spatial organization is engineered at the molecular level. This class of materials can be defined as nano. They are made of assembled nanosized objects or molecules. Their macroscopic behavior arises from the combination of the novel properties of the individual building blocks and their mutual interaction. Nanoscale materials frequently show a behavior which is intermediate between that of a macroscopic solid and that of an atomic or molecular system. Consider for instance the case of an inorganic crystal composed of very few atoms. Its properties will be different from that of a single atom, but we cannot imagine that they will be the same as those of a bulk solid. The number of atoms on its surface, for instance, is a significant fraction of the total number of atoms, and therefore will have a large influence on the overall properties of the crystal. We can easily imagine that this crystal might have a higher chemical reactivity than the corresponding bulk solid and that it will probably melt at lower temperatures.

From the point of view of a chemist, the basic building blocks of matter are atomic nuclei and electrons. In an atom, electrons orbit around a single nucleus, whereby the number of electrons depends on the element. In the simplest case, the hydrogen atom, one electron orbits around one proton. The electronic states of the hydrogen atom can be calculated analytically.[38,39] As soon as more than one electron is involved, however, the calculation of the energy levels becomes more complicated, since in addition to the interaction between nucleus and electron now also electron-electron interactions have to be taken into account. Although the energy states of many-electron atoms

cannot be derived analytically anymore, approximations such as the Hartree-Fock method exist.[39] Each electron can be ascribed to an individual orbit, called atomic orbital (AO), with an associated discrete energy level. Depending on the angular moment of the orbit, AOs have spherical (s-orbital), club-like (p-orbital) or a more complicated (d-,f-orbitals) shape. The eight valence electrons of a Neon atom, for example, occupy one s- and three p-orbitals around the nucleus, one spin up and one spin down per orbit 10, whereby the energy level of the s- is lower than that of the p-orbitals. Following the rules of quantum mechanics the energy levels are discrete. The next bigger structure obtained from the combination of several atoms is the molecule. Now electrons orbit collectively around more than one nucleus. In a molecule, electrons which are responsible for the covalent bonds between individual atoms cannot be any longer ascribed to one individual atom, but they are "shared". In methane (CH_4), for instance, each of the four sp^3 atomic orbitals of the central carbon atom is linearly combined with the s orbital of a hydrogen atom to form a bonding (s) and an anti-bonding (s*) orbital, respectively.[38] Since these orbitals are "shared" between the atoms they are called molecular orbitals (MO), see Figure 1. Only the lowest energy (bonding) orbitals are occupied and this explains the relative stability of methane.[39] With the same principle it is possible to derive the electronic structure of more complex systems, such as large molecules or atomic clusters. When combining atoms to form a molecule, we start from discrete energy levels of the atomic orbitals and we still end up obtaining discrete levels for the molecular orbitals.[38]

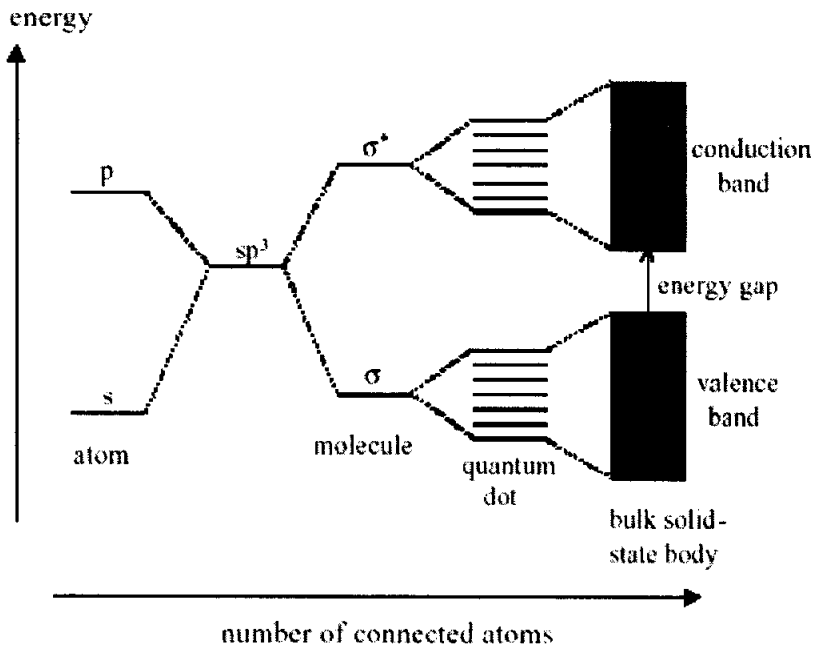

Figure 2 Electronic energy levels depending on the number of bound atoms. By binding more and more atoms together, the discrete energy levels of the atomic orbitals merge into energy bands (here shown for a semiconducting material).[40]

Colloidal quantum dots : Colloidal quantum dots are remarkably different from the quantum dot systems mentioned above as they are chemically synthesized using wet chemistry and are free-standing nanoparticles or nanocrystals grown in solution.[41] In this case, colloidal quantum dots are just a subgroup of a broader class of materials that can be synthesized at the nanoscale using wet chemical methods. In the fabrication of colloidal nanocrystals, the reaction chamber is a reactor containing a liquid mixture of compounds that

control the nucleation and the growth. In a general synthesis of quantum dots in solution, each of the atomic species that will form the nanocrystal building blocks is introduced in the reactor as a precursor. A precursor is a molecule or a complex containing one or more atomic species required for growing the nanocrystal. Once the precursors are introduced in the reaction flask they decompose, forming new reactive species (the monomers) that will cause the nucleation and the growth of the nanocrystals. The energy required to decompose the precursors is provided by the liquid in the reactor, either by thermal collisions or by a chemical reaction between the liquid medium and the precursors, or by a combination of the two mechanisms.[42] The key parameter in the controlled growth of colloidal nanocrystals is the presence of one or more molecular species in the reactor, broadly termed here as surface molecule that is dynamically adsorbed to the surface of the growing quantum dot under the reaction conditions. It must be mobile enough to provide access for the addition of monomer units, while stable enough to prevent the aggregation of nanocrystals. The choice of surfactants varies from case to case: a molecule that binds too strongly to the surface of the quantum dot is not suitable, as it would not allow the nanocrystal to grow. On the other hand, a weakly coordinating molecule would yield large particles, or aggregates.[43] Some examples of a suitable surfactant include for instance alkyl thiols, phosphines, phosphine oxides, phosphates, phosphonates, amides or amines, carboxylic acids, and nitrogen-containing aromatics. If the growth of nanocrystals is carried out at high temperatures (for instance at 200 - 400 ℃) then the surfactant molecules must be stable at such conditions in order to be a suitable candidate for controlling the growth.

History and development of Langmuir-Blodgett films : The effects of oils on water surfaces have been known for many centuries. Babylonians in the eighteenth century BC have been recorded as practising divinity by observing the effects of oils spread on water. The Japanese printing art of Sumi-Nagashi (black-ink-let-flow) is one of the first technical applications of floating monolayers. The first scientific interest in mono-molecular layers was shown by Benjamin Franklin (during a visit to London to discuss certain colonial matters) when he spread oils onto the pond at Clapham Common and observed that the one teaspoon full of oil which he used had a calming influence over half an acre of water. Modern investigations of molecular films began with Agnes Pockels experimenting with a very simple trough in her kitchen. Her ideas, expressed as letters to Lord Rayleigh, were published in 'Nature' in 1891. She realized the importance of cleanliness and developed many of the techniques which are regarded as standard today. Her experiments included the first containment of a monolayer by means of a barrier. Further investigations carried out by Rayleigh, Devaux and Hardy confirmed the monomolecular nature of such films. However it was Irving Langmuir who contributed the greatest advances. Langmuir studied the pressure-area relationship of molecules on an aqueous surface. Katherine Blodgett, who worked with Langmuir on the properties of floating monolayers, developed the technique of transferring the films onto solid substrates and hence building up multilayer films. Recently many possible applications of Langmuir-Blodgett films in the fields of electronics, optics, molecular electronics and biotechnology are currently being investigated by research groups throughout world.

Langmuir films : Langmuir films consist of surface active materials or surfactants trapped at the interface between two dissimilar phases. Surfactants are molecules which are amphiphilic, which are composed of a hydrophilic part and a hydrophobic part. Hydrophilic groups consist of groups such as carboxylic acid, sulphates, amines and alcohols. When surfactants, dissolved in a non-aqueous volatile solvent, are introduced onto a polar liquid surface, the solvent will be evaporated and leaving the surfactants oriented at the liquid-gas interface-the hydrophilic head groups pulling the molecule into the bulk of the water and the hydrophobic tail groups pointing into the air. A surface monolayer will only be achieved if the amphiphatic balance of the molecule is correct; that is the balance between hydrophobic and hydrophilic parts. If the hydrophobic tail group is too short (not hydrophobic enough) the molecule will be dragged into the water and will dissolve while if there is no hydrophilic part, the molecules may form thicker multi-layer films on the surface or even evaporate. Sweeping a barrier over the water surface causes the molecules to come closer together and eventually to form a compressed, ordered monolayer. The film produced by such a method is known as a Langmuir film.

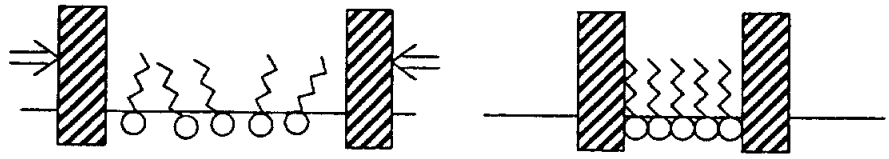

Figure 3 Schematic drawings of expanded and compressed monolayers on a water surface.

The Langmuir-Blodgett technique : Langmuir-Blodgett films consist of mono-molecular layers stacked sequentially onto a solid substrate. A suitably treated substrate is lowered into the water, breaking through the Langmuir film and, provided the substrate surface is of the right type, the Langmuir film attaches itself to the substrate, coating it in a mono-molecular layer. Once the first layer has been deposited, further layers will be deposited on each subsequent pass of the substrate through the air/water interface. Multilayers can therefore be deposited to produce a film the thickness of which is the product of the individual molecular chain length and the number of times that the substrate has crossed the air/water interface. Two types of substrates can be coated - hydrophobic and hydrophilic. A hydrophobic substrate will result in deposition on the first down pass, the hydrophobic hydrocabon tails adhering to the hydrophobic substrate. With hydrophilic substrate no ordered deposition will occur until the first up-stroke because the hydrophobic tails are repelled by the hydrophilic substrate as it is immersed in the water. Generally, if the direction of the meniscus at the water/substrate boundary follows the direction of substrate movement, deposition will occur.

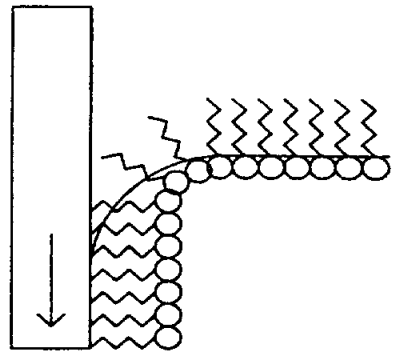

Figure 4 Schematic drawings of deposition of the first monolayer onto a hydrophobic substrate.

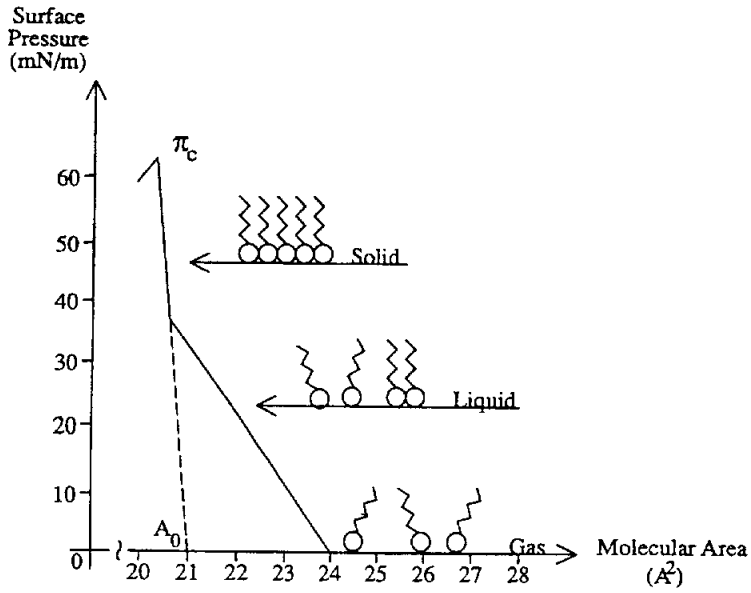

Figure 5 Pressure-area isotherm of a fatty acid on the pure water surface.

Pressure-area isotherm : Molecules in a solution are subject to attractive forces; in the bulk of the solution these forces are equal. However, at a surface or interface the forces are unequal and the net effect is to pull the peripheral molecules into the bulk of the solution. This effect gives rise to surface tension. The surface tension can be defined as the work required to expand the surface isothermally by unit area. The tendency of surface-active molecules to accumulate at interfaces favours expansion of the interface and hence lowers the surface tension. Such behaviour makes it possible to monitor the surface pressure as a function of the area occupied per molecule provided that the number of molecules deposited on the surface is known.

Photoluminescence : Multilayer material systems are increasingly important in the development of smaller, faster, and more efficient electronic and optoelectronic devices. The primary motivation for using multilayer structures is to change the potential energy of electrons and holes at the material interfaces. Because phenomena at surfaces and interfaces tend to dominate the behavior of excitations in these heterostructures, the performance of many microelectronic devices is limited by the nature of heterojunctions. Smooth and atomically abrupt interfaces are necessary for good optical and electrical reflection, uniform quantum confinement, and high carrier mobility. Even more importantly, defects and impurities at interfaces provide new states for electrons and holes, altering their motion, lifetime, and transition energies. When light of sufficient energy is incident on a material, photons are absorbed and electronic excitations

are created. Eventually, these excitations relax and the electrons return to the ground state. If radiative relaxation occurs, the emitted light is called PL. This light can be collected and analyzed to yield a wealth of information about the photoexcited material. The PL spectrum provides the transition energies, which can be used to determine electronic energy levels. The PL intensity gives a measure of the relative rates of radiative and nonradiative recombination. Variation of the PL intensity with external parameters like temperature and applied voltage can be used to characterize further the underlying electronic states and bands.

PL depends on the nature of the optical excitation. The excitation energy selects the initial photoexcited state and governs the penetration depth of the incident light. The PL signal often depends on the density of photoexcited electrons, and the intensity of the incident beam can be adjusted to control this parameter. When the type or quality of material under investigation varies spatially, the PL signal will be changed with excitation position. In addition, pulsed optical excitation provides a powerful means for studying transient phenomena. Short laser pulses produce virtually instantaneous excited populations, after which the PL signal can be monitored to determine recombination rates. Because PL often originates near the surface of a material, PL analysis is an important tool in the characterization of surfaces. The utility of PL for this purpose is derived from its unique sensitivity to discrete electronic states, many of which lie near surfaces and interfaces. Using the techniques noted above, the nature of these states can be probed in detail. The energy distribution and density of interface states can be ascertained by studying the excitation intensity dependence of the PL spectrum. The presence of

surface adsorbates alters the intensity of the PL signal. When the states serve as long-lived traps, the depth of the trap can be determined by observing thermal activation in temperature-dependent PL. In fact, even if interface states are nonradiative, which is usually the case, the states alter the time-resolved PL of radiative transitions in the material. Nonradiative traps dominate the transient PL signal at low carrier density.

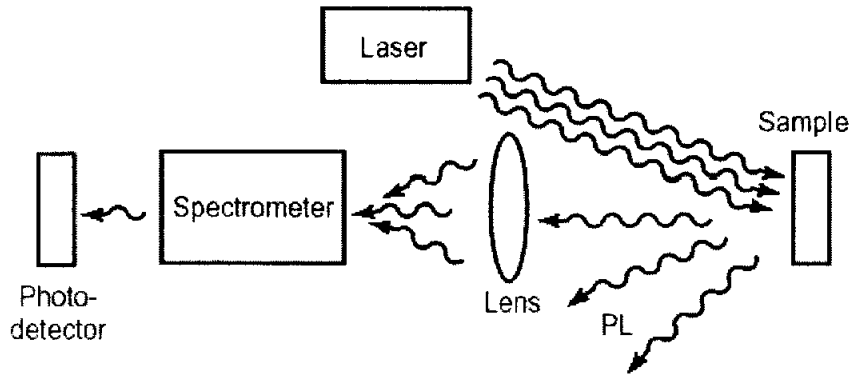

Figure 6 Typical experimental set-up for PL measurements.

PL is simple, versatile, and nondestructive. The instrumentation that is required for ordinary PL work is modest: an optical source and an optical power meter or spectrophotometer. A typical PL set-up is shown in Figure 5. Because the measurement does not rely on electrical excitation or detection, sample preparation is minimal. This feature makes PL particularly attractive for material systems having poor conductivity or undeveloped contact/junction technology. Measuring the continuous wave PL intensity and spectrum is quick

and straightforward. On the other hand, investigating transient PL is more challenging, especially if recombination processes are fast. Instrumentation for time-resolved detection, such as single photon counting, can be expensive and complex. Even so, PL is one of the only techniques available for studying fast transient behavior in materials.

That is, PL is the optical emission obtained by photon excitation (usually a laser) and is commonly observed with III-V semiconductor materials. This type of analysis allows non-destructive characterization of semiconductors (material composition, qualitative investigations, etc.) PL spectroscopy is a contactless, nondestructive method of probing the electronic structure of materials. Light is directed onto a sample, where it is absorbed and imparts excess energy into the material in a process called "photo-excitation." One way this excess energy can be dissipated by the sample is through the emission of light, or luminescence. In the case of photo-excitation, this luminescence is called "photoluminescence". The intensity and spectral content of this PL is a direct measure of various important material properties.

2-2-2. Experimental technique

The synthetic procedure is a modified version of the method for the synthesis of monodisperse nanoparticles, which empolys the formation of a metal-surfactant complex followed by aging at high temperature. To identify properties of the synthesized nanoparticles and nanocomposites, we made various experiments. The crystal structures of the synthesized nanoparticles were identified by using X-ray powder diffraction (XRD), Philps XPert-MPD system. The size and shape of nanoparticles were obtained by transmission electron microscopy (TEM) by using a Jeol, JEM-2010. Samples for TEM samples were prepared on 300 mesh copper grids coated with carbon. A drop of CdS or CdSe nanoparticle solution was carefully placed on the copper grid surface and dried. The optical properties of the CdS and CdSe nanoparticles have been characterized by absorption and photoluminescence spectroscopy. UV-vis absorption and transmission spectra of the synthesized CdS or CdSe nanoparticles were taken by using a Varian, Cary 1C. Photoluminescence (PL) spectra were recorded on a Perkin-Elmer, LS50B to know the wavelength of excitation and emission. The Langmuir-Blodgett film of surfactant/CdS nanoparticle was prepared by transferring monolayer by using the Langmuir-Blodgett technique. The Langmuir trough for pressure-area isotherm experiment (45 cm x 15 cm, KSV model 2200) is housed within a large Plexiglas box to isolate it from laboratory atmosphere. The trough must be carefully placed to ensure that it was completely level and that there was a good seal between trough and barrier; this is essential to the monolayer compression. The Langmuir-Blodgett film of surfactant/CdS nanoparticle was characterized by TEM,

thermogravimetric analysis (TGA) and atomic force microscopy (AFM). The sample was measured by using TGA, Perkin-elmer (U.S.A). The sample of AFM of Langmuir-Blodgett film of surfactant/CdS nanoparticle was prepared by transferring onto mica surface. AFM image was obtained with Digital Instruments (U.S.A), Multi-ModeTM SPM.

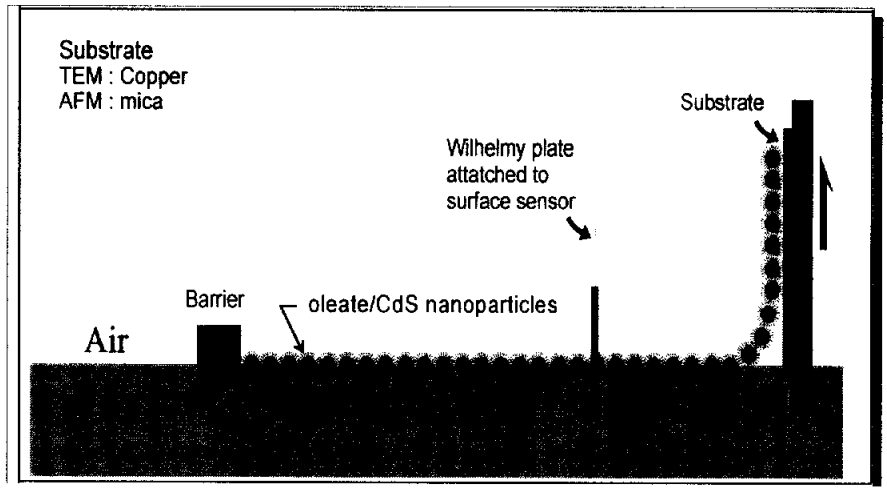

Figure 7 Schematic drawings of Langmuir-Blodgett deposition of oleate/CdS nanoparticle complex monolayer at the air/water interface.

3. Result and Discussion

3-1. Characterization of CdS and CdSe nanoparticles

3-1-1. X-ray powder diffraction (XRD) study

XRD technique which can be used for identification of rock or mineral content of powder samples, or determination of the chemical structure of crystalline materials. This technique can also be used for identification of any crystalline material. Using XRD, a diffraction pattern is produced for each crystalline sample. This diffraction pattern is unique for each and every crystalline material, like a finger-print. Figure 7 shows the X-ray powder diffraction (XRD) pattern of the synthesized nanoparticles. The XRD patterns showed that the crystallinites of the samples. All the peaks of CdS in Figure 6 were indexed as the cubic structure of CdS, which are consistent with the reported data for CdS (JCPDS Card File No. 80-0019). The CdSe diffraction patterns exhibit peak positions corresponding to their cubic structures (JCPDS Card File No. 19-0191). The CdSe diffraction patterns exhibit peak positions corresponding to their cubic structures (JCPDS Card File No. 19-0191).

3-1-2. Transmission electron microscopy (TEM)

Materials for TEM must be specially prepared to thicknesses which allow electrons to transmit through the sample, much like light is transmitted through materials in conventional optical microscopy. Because the wavelength of electrons is much smaller than that of light, the optimal resolution attainable for TEM images is many orders of magnitude better than that from a light microscope. Thus, TEM can reveal the finest details of internal structure - in some cases as small as individual atoms. Magnifications of 350,000 times can be routinely obtained for many materials. The energy of the electrons in the TEM determine the relative degree of penetration of electrons in a specific sample, or alternatively, influence the thickness of material from which useful information may be obtained. TEM is a complementary tool to conventional crystallographic methods such as X-ray diffraction.

TEM images of Figure 7 were collected on a JEM 2010 with 200 kV accelerating voltage. Samples were prepared by evaporation of the colloidal solution onto a 300 mesh Cu grid. TEM was employed to obtain direct information on the size and shape of the produced nanoparticles. The TEM images in Figure 7 show the CdS (a) and CdSe (b) nanoparticles with diameters of 2.6 - 7.8 nm and 6 - 13 nm, respectively. The particle shape is spherical and triangle. Especially, the triangle shape is made by synthetic conditions of high temperature and pressure.

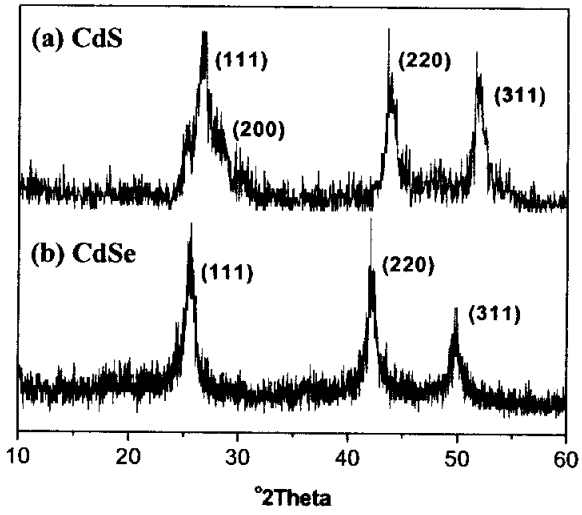

Figure 8 X-ray powder diffraction (XRD) patterns of CdS and CdSe nanoparticles. These nanoparticles are capped with oleate as a surfactant.

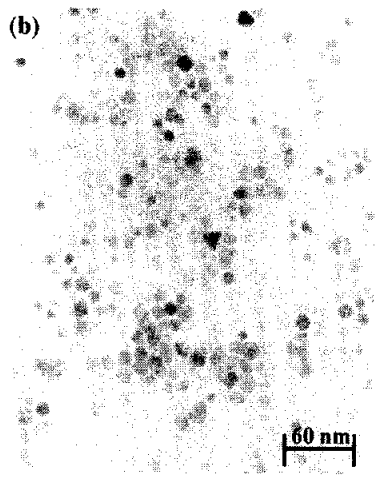

Figure 9 Transmission electron microscopy (TEM) images of (a) CdS and (b) CdSe nanoparticles.

3-1-3. High Resolution transmission electron microscopy (HRTEM)

Figure 9 shows TEM lattice images for one particle indicating highly crystalline structure. In Figure 9 (a) and (b), CdS lattice spacing of 1.6774 Å and 2.0545 Å was consistent with the lattice spacing between (222) and (220) planes. In the lattice spacing of Figure 9 (c) and (d), CdSe was measured carefully as 3.51 Å and 2.149 Å. This is consistent with the lattice spacing between (111) and (220) planes for cubic CdSe.

3-1-4. Electron diffraction (ED)

Electron diffraction (ED), in its simplest application, is used to identify crystalline substances based on the spacing of atomic planes within their structures. ED provides similar structural information as neutron diffraction. Electron beams strongly interact with nuclei. The strong interaction of electrons with matter results in a low penetration depth, and electron diffraction is usually used in a reflection geometry to study surfaces or thin films. Electron beams are easy to manipulate, detect, and focus to small spots to provide high spatial resolution. Further analysis of ED patterns can provide key information on orientation relationships between crystalline phases (such as coatings on substrates, precipitates in materials, etc.), the nature of defects in solids, order-disorder effects, and crystallite size analysis. Electrons scatter from gases and electron diffraction must be performed under vacuum. ED is usually carried out in a TEM.

Figure 10 shows an example of electron diffraction pattern from CdS and CdSe nanoparticles. From the rich information in this pattern, we can take a considerable improvement of characterizing nanoparticles. The diffraction rings can be indexed to (200), (311) and (400) planes at CdS nanoparticle corresponding to XRD data of CdS. In case of the obtained data was indexed to (111), (220) and (311) planes. The same result is observed for XRD spectra of Figure 7.

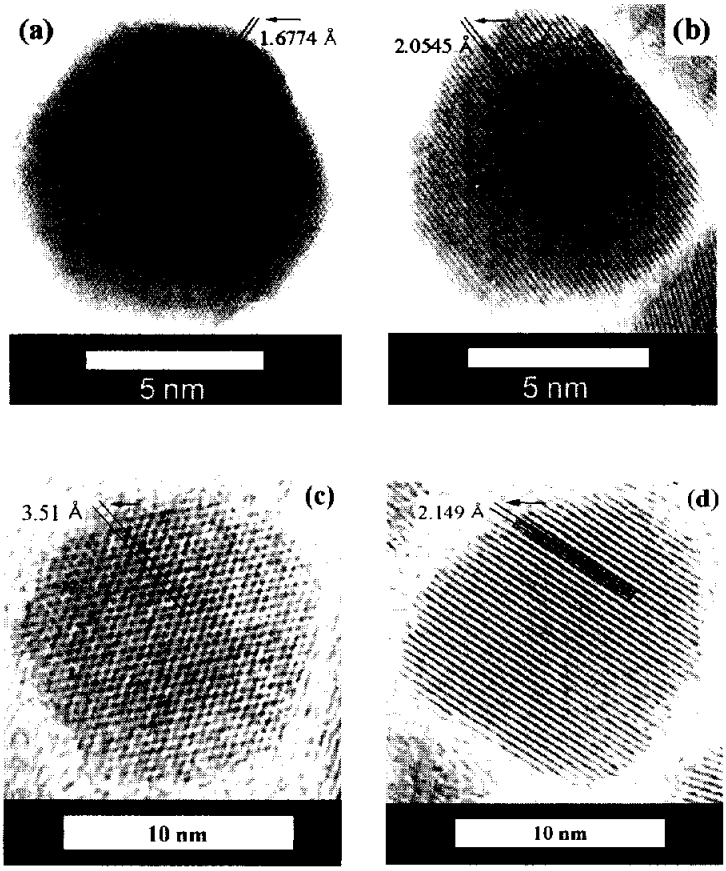

Figure 10 High resolution transmission electron microscopy (HRTEM) lattice images of (a) and (b) of CdS and (c) and (d) of CdSe nanoparticles.

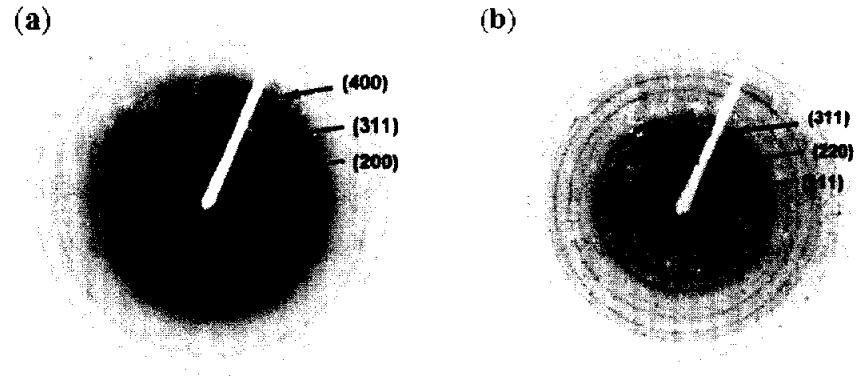

Figure 11 Electron diffraction (ED) patterns of (a) CdS and (b) CdSe nanoparticles.

3-1-5. Energy dispersive X-ray (EDX) spectrometer

Elemental analysis is achieved by collecting the X-rays generated when the incident electron beam interacts with the atoms of the sample. Each element in the sample produces X-rays with characteristic energies whose peak intensities are related to the amount of the elements present. The energies of these X-ray photons are converted into electrical signals in a Si (Li) detector and are processed to produce an intensity spectrum in counts per second. The technique is able to resolve all of the elements from boron or sodium to uranium. When the beam energy exceeds the critical x-ray ionization energy for a shell or subshell so that it is ionized, all possible transitions involving that ionized shell may take place, producing a family of peaks, which will become more complicated as the electronic structure of the atom increases in complexity. The

analyst must be familiar with the concept of a family of x-ray peaks.

Figure 11 shows the EDX spectra of the CdS and CdSe nanoparticles excited by an electron beam (200 kV). Peaks for the elements of Cd and S were observed together with O and Cu. The O and Cu peaks are due to the EDX detector and Cu grid, respectively. The EDX measurement indicate the presence of Cd and S in samples, with the Cd : S ratios 50.31 : 49.69 being very close to 1:1. Element analysis for the samples of CdSe in Figure 10 gives Cd : Se atomic ratios of 52.78 : 47.22, which is close to 1:1. There is no impurity atom of the nanocrystallites. From the electron diffraction pattern and the EDX spectra, we could confirm that the CdS or CdSe nanoparticles in TEM images are pure materials.

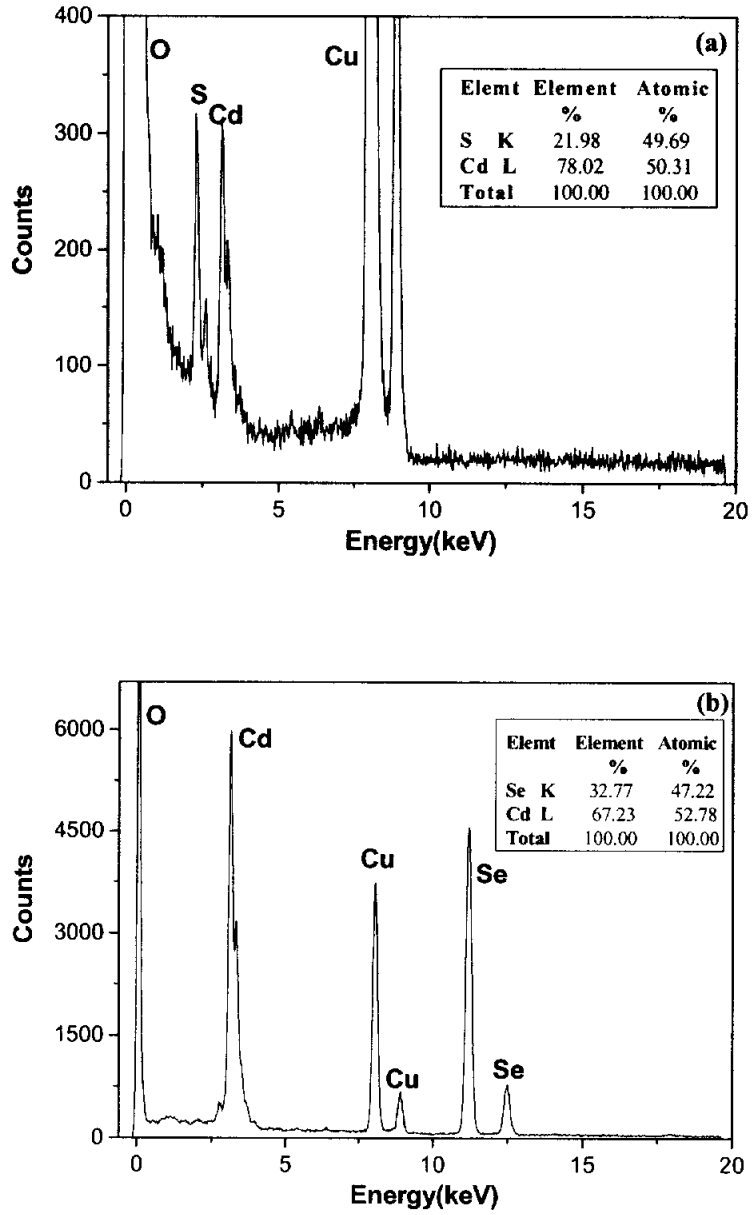

Figure 12 Energy dispersive X-ray spectra of (a) CdS and (b) CdSe nanoparticles.

3-1-6. UV-vis study

Figure 12 presents UV-vis absorption spectra of CdS or CdSe nanoparticles prepared in aqueous solutions. Sodium oleate has been used as effective stabilizer for the synthesis of CdS and CdSe nanoparticles. The absorption spectrum in Figure 11 displays an absorption peak at 500 nm for CdS nanoparticles. Compared with the band gap of the characteristic absorption (> 500 nm) of bulk CdS, a blue-shift to 490 nm is indicative of size quantization.[44,45] The UV-vis spectrum of the synthesized CdSe nanoparticles had no peculiar characteristics. This is caused by the broad particle size distribution.

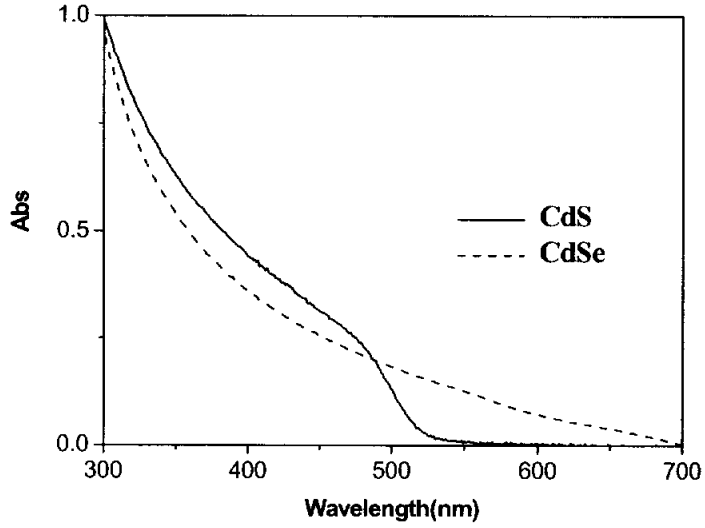

Figure 13 UV-vis spectra of CdS and CdSe nanoparticles.

3-1-7. Photoluminescence (PL) study

The photoluminescence (PL) spectra were obtained with and excitation wavelength at 360 nm. PL studies of the synthesized nanoparticles indicated excitonic transition. The line shape of the PL spectrum is essentially given by the inhomogeneous broadening which is due to the size distribution of the crystallites. The PL spectrum in Figure 13 shows a narrow emission band at 490 - 530 nm. A narrow PL band at 512 nm was observed. The CdS nanoparticles stabilized with oleate showed PL emission at lower wavelengths corresponding to somewhat smaller size of particles. Thus, the use of sodium oleate as stabilizing agent allows the synthesis of highly crystalline CdS nanoparticles. This is well shown by strong band-edge of PL. The fluorescence and transient absorption kinetics are extremely sensitive to surface to surface defects.[46-49] The theory was explained by high-energy luminescence (superradiant luminescence) due to the band gap emission which is observed only under certain conditions (size and temperature dependent) with a lifetime of a few picoseconds.[50] The photoluminescence spectrum of CdSe showed an emission with maximum at 600 nm (λ_{ex} = 365 nm), which shows an obvious blue-shift compared with that of the bulk material.[51,52] In chemistry, size-dependent optical properties of colloidal semiconductor particles have been observed since the beginning of the last century (for instance in CdS colloids,[53] although it was only toward its end[54] that this fact was rationalized in terms of size quantization. The most striking effect in semiconductor nanoparticles is the widening of the gap Eg between the highest occupied electronic states (the top of the

original valence band) and the lowest unoccupied states (the bottom of the original conduction band).[55] This directly affects the optical properties of quantum dots as compared to the corresponding bulk material. The minimum energy needed to create an electron-hole pair in a quantum dot (an exciton) is defined by its band gap (Eg). Light with energy lower than Eg cannot be absorbed by the quantum dot. Since the band gap depends on the size of a quantum dot, the onset of absorption is also size-dependent.[56,57]

In Figure 13 we show that smaller quantum dots have an absorption spectrum that is shifted to shorter wavelengths with respect to larger quantum dots and to the bulk case. Excitons in semiconductors have a finite lifetime due to the recombination of the photoexcited electron-hole pair. In quantum dots, the energy released upon exciton annihilation is too large to be dissipated by vibrational modes. Instead, it is released in the form of emitted photons. Radiative decay through emission of photons, in other words fluorescence, is a highly probable decay channel in quantum dots.[58]

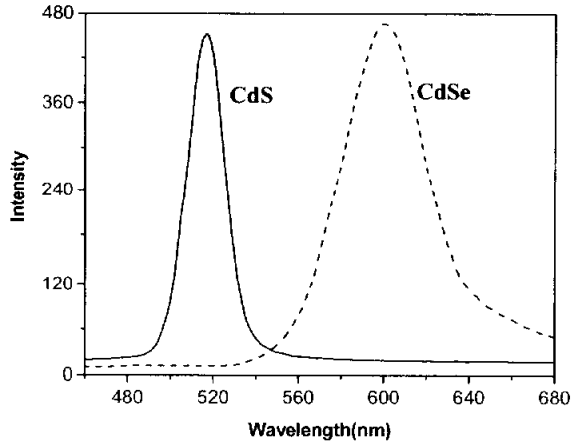

Figure 14 Photoluminescence spectra of CdS and CdSe nanoparticles.

3-1-8. Photoluminescence images

These photoluminescence images were obtained by digital camera. The synthesized CdS or CdSe nanoparticles were dissolved in iso-octane. Before UV irradiation, the color of CdS or CdSe nanoparticles solution was yellow and brown, respectively. The light of 365 nm was irradiated by UV lamp. Then, the color of each solution was changed to green and orange, respectively. These data backed up the previous PL results.

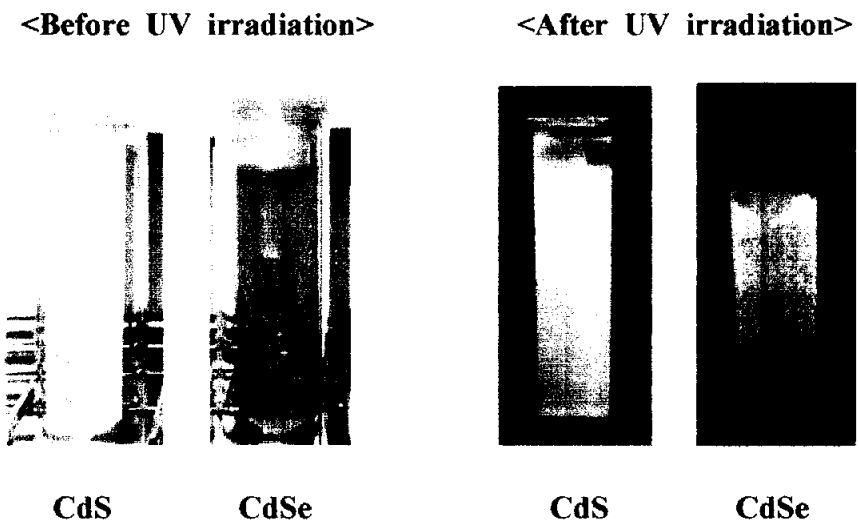

Figure 15 Photoluminescence images of CdS and CdSe solutions according to irradiation of UV lamp (solvent : iso-octane).

Wavelength (nm)	Color
340 - 400	below UV wavelength
400 - 430	violet
430 - 500	blue
500 - 560	green
560 - 620	yellow - orange
620 - 700	orange - red
Above 700	above IR wavelength

Table 1 Wavelength color according to wavelength range of 340 - 700 nm.

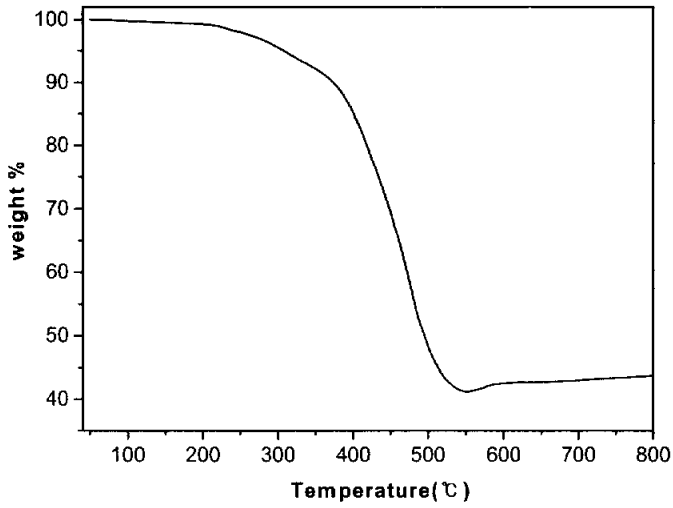

Figure 16 TGA graph of CdS nanoparticles containing oleate.

3-2. Coverage calculation of CdS surrounding with organic surfactant

3-2-1. Thermogravimetric analysis (TGA)

TGA is a thermal analysis technique used to measure changes in the weight (mass) of a sample as a function of temperature and/or time. The measurements provide basic information about the thermal stability of a chemical and its composition. Precise measurement of the weight change of a solid as it is heated at a controlled rate can be used, for example to determine the amount of chemically attached water or the organic content of an otherwise inorganic substance. TGA is one of the most commonly requested thermal techniques and it is used to characterize both inorganic and organic materials, including polymers. TGA is commonly used to determine polymer degradation temperatures, residual solvent levels, absorbed moisture content, and the amount of inorganic (noncombustible) filler in polymer or composite material compositions. A simplified explanation of a TGA sample evaluation may be described as follows. A sample is placed into a tared TGA sample pan which is attached to a sensitive microbalance assembly. The sample holder portion of the TGA balance assembly is subsequently placed into a high temperature furnace. The balance assembly measures the initial sample weight at room temperature and then continuously monitors changes in sample weight (losses or gains) as heat is applied to the sample. TGA tests may be run in a heating mode at some controlled heating rate, or isothermally. Typical weight loss profiles are analyzed for the amount

or percent of weight loss at any given temperature, the amount or percent of noncombusted residue at some final temperature, and the temperatures of various sample degradation processes.

Figure 15 shows the TGA curves of CdS nanoparticles containing oleate. The prepared sample was heated from 50 ℃ to 800 ℃ at regular intervals of 10 ℃ per minute in the atmosphere. The decomposition of surfactant/CdS nanoparticles proceeds at 250 - 350 °C. This graph revealed the ratio of decomposed oleate and existent inorganic CdS nanoparticles. That is, the ratio of oleate and CdS nanoparticles in the sample was 59 and 41%, respectively.

3-2-2. Surface pressure-area isotherm

A 1 mg of CdS nanoparticles containing oleate were dissolved in 1 ml of chloroform. Then, 30 ml of the prepared sample was sprayed on pure water surface using microsyringer. By moving barrier, we can obtain data of surface pressure-area isotherm.

Figure 16 shows the pressure-area isotherm of oleate/CdS nanoparticles at the air/water interface. The used oleate/CdS nanoparticles resulted in the stable monolayer at the air/water interface. The limiting areas of monolayers of oleate/CdS nanoparticles was 172 cm^2. The gram of oleate molecule is 1.77×10^{-5} g by value of TGA data and then mole of oleate is 6.288×10^{-8} mol. Thus, oleate molecule has a number of 3.78×10^{16} by these data.

From the pressure-area isotherm of stearic acid in Figure 17, we can calculate one molecular area of stearic acid. A 2 mM of stearic acid in water had area of 166 cm^2 when monolayer was formed. The

mole of used stearic acid is 5.9×10^{-7} mol. Thus, stearic acid has molecule number of 3.55×10^{17} and one molecular area of stearic acid is 4.676×10^{-2} nm^2 by value of surface pressure-area isotherm. The surface area of CdS sphere having average diameter of 7.8 nm is 191 nm^2. That is, stearic acid's whole number in CdS sphere surface area is 4085. Therefore, number of oleate molecule that is covering CdS surface is 4085 in case of ideal state.

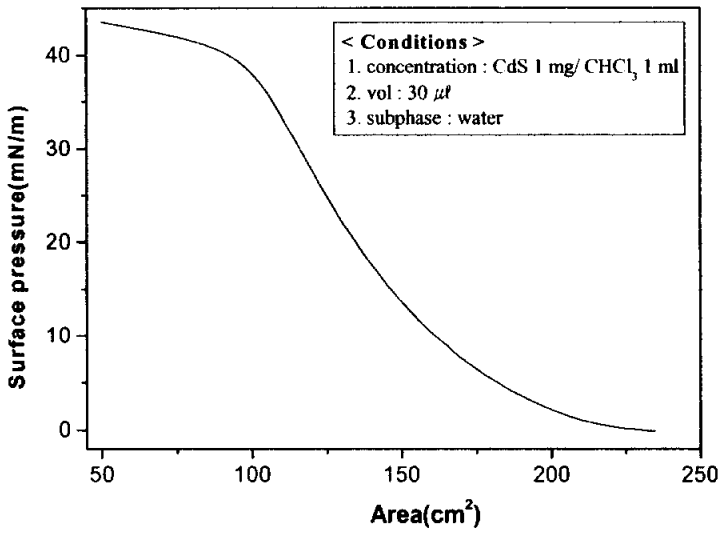

Figure 17 Surface pressure-area isotherm of CdS nanoparticles containing oleate in the subphase of pure water at room temperature.

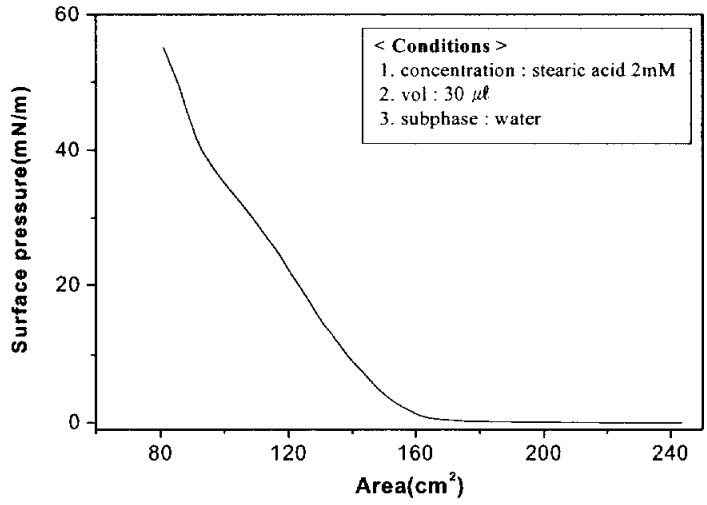

Figure 18 Surface pressure-area isotherm of stearic acid in the subphase of pure water at room temperature.

3-2-3. Coverage calculation

The length of oleate molecule is 1.25 nm and diameter of CdS nanoparticle is 7.8 nm. Thus, whole diameter of CdS nanoparticle surrounding oleate is about 10.3 nm as Figure 18. CdS nanoparticle has area of 106.09 nm^2. In consequence, whole number of CdS nanoparticles is 1.62×10^{14} by 172 nm^2 value of oleate/CdS nanoparticle in Figure 16.

That is, number of CdS nanoparticles and oleate molecules is 1.62 $\times$ 10^{14} and 3.78 $\times$ 10^{16}, respectively in the previous data. The number of oleate molecule that adhere per one CdS nanoparticle is 233. That is to say, 233 of oleate molecule was attached on one molecular CdS nanoarpticle. In view of the results so far achieved, stearic acid's whole number in surface of CdS sphere is 4085. In case of the synthesized CdS nanoparticles, but CdS has 233 of oleate molecule. we can know that oleate molecule is enclosing about 5.7% on the CdS surface.

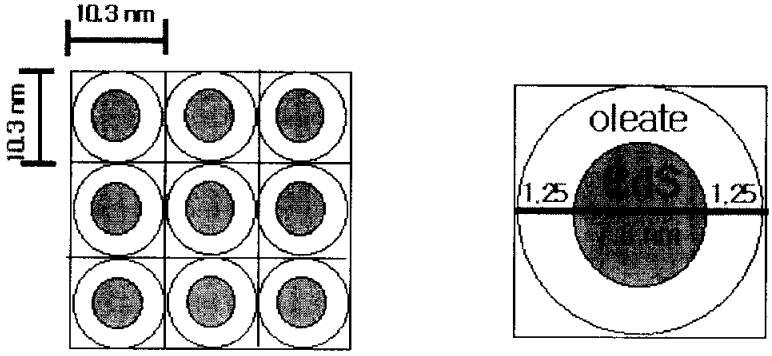

Figure 19 Schematic drawings of oleate/CdS nanoparticles for coverage calculation.

3-2-4. Transmission electron microscopy (TEM)

The dispersion of CdS nanoparticles in the Langmuir-Blodgett film was studied with TEM image as shown in Figure 19. The TEM image of the films deposited 2 layers onto the 300 mesh formvar coated copper grid at 25 mN/m surface pressure shows the almost homogeneous dispersion. Most of the CdS nanoparticles are spherical having diameters of 5.7 - 11.7 nm. The homogeneously dispersed CdS nanoparticles resulted in a single domain of an isolated particle.

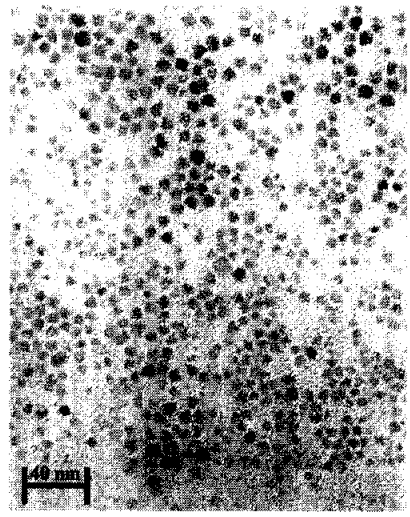

Figure 20 Transmission electron microscopy (TEM) image of Langmuir-Blodgett film of CdS nanoparticles by Langmuir-Blodgett technique.

3-2-5. Atomic force microscopy (AFM)

The atomic force microscopy (AFM) is being used to solve processing and material problems in a wide range of technologies affecting the electronics, telecommunications, biomedical, chemical, automotive, aerospace, and energy industries. The materials under investigation include thin and thick film coatings, ceramics, composites, glasses, synthetic and biological membranes, metals, polymers, and semiconductors. The AFM is being applied to studies of phenomena such as abrasion, adhesion, cleaning, corrosion, etching, friction, lubrication, plating, and polishing. AFM images show critical information about surface features with unprecedented clarity. The AFM can examine any rigid surface, either in air or with the specimen immersed in a liquid. "Minor" (and major) differences between "smooth" surfaces are shown dramatically. On one hand, the AFM can resolve very tiny features, even single atoms, that were previously unseen. On the other hand, the AFM can examine a field of view larger than 125 microns (0.005 inch), so that you can make comparisons with other information. The AFM can also examine rough surfaces, since its vertical range is more than 5 microns.

The image of the nanocomposite film of oleate/CdS nanoparticles obtained by atomic force microscopy (AFM) is shown in Figure 21 and 22. The surface morphology of mica used as a solid substrate for the film deposition was comparatively scanned before deposition. The Langmuir-Blodgett film of oleate/CdS nanoparticles was scanned with the contact mode AFM. In Figure 21, the surface image (a) and three-dimensional surface morphology (b) of Langmuir-Blodgett film of

oleate/CdS nanoparticles deposited onto mica surface at 25 mN/m surface pressure with two layers obtained with AFM. These shown images were not good because of aggregation of used organic surfactant. The mica substrate was deposited by Langmuir monolayer of oleate/CdS nanoparticle complex from the air/water interface by Langmuir-Blodgett technique at 15 mN/m surface pressure as shown Figure 22. The scan area of a two-layered Langmuir-Blodgett films of oleate/CdS nanoparticles is 1.00 × 1.00 μm and the scan speed is 5 Hz. Even on this large scale the surface morphology shown by AFM image gives the well formed surface structure compared with Figure 21. Consequently, we couldn't get satisfied results because Lagmuir-Blodgett films of oleate/CdS nanoparticles at higher surface pressure had aggregated organic surfactants.

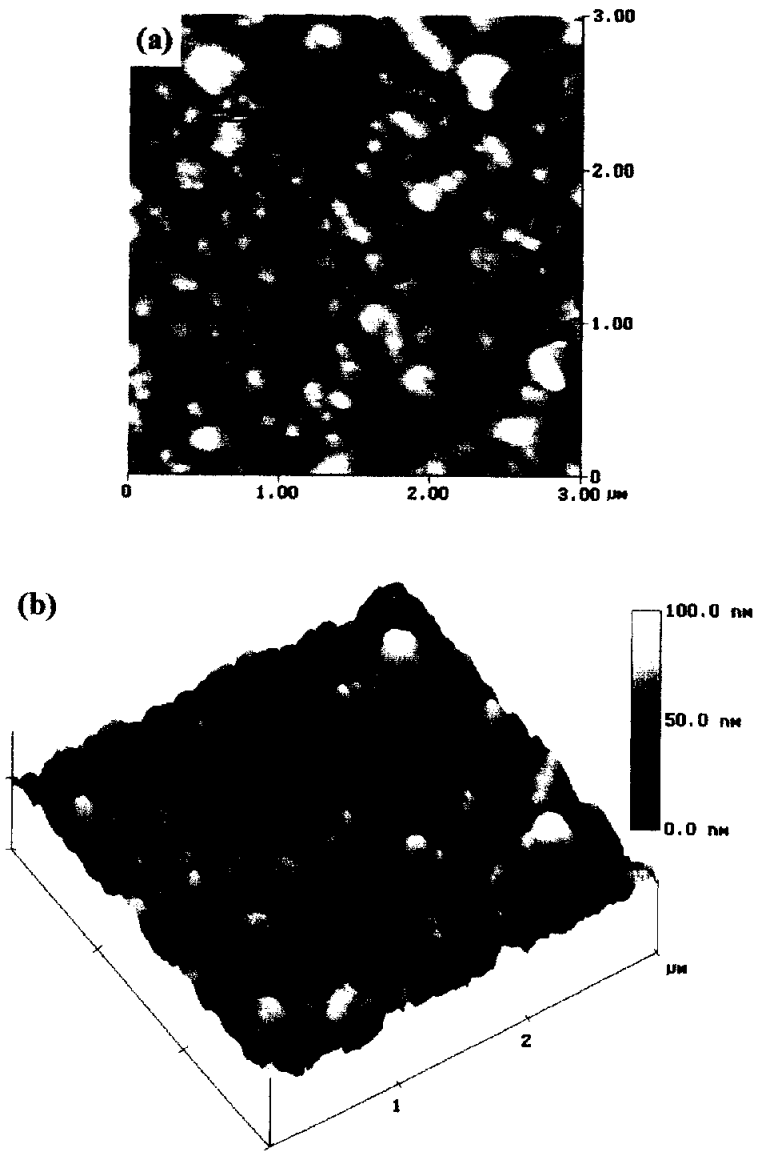

Figure 21 Top view on the surface image (a) and three-dimensional surface morphology (b) of Langmuir-Blodgett film of CdS nanoparticle deposited onto mica surface at 25 mN/m surface pressure with two layer obtained with AFM.

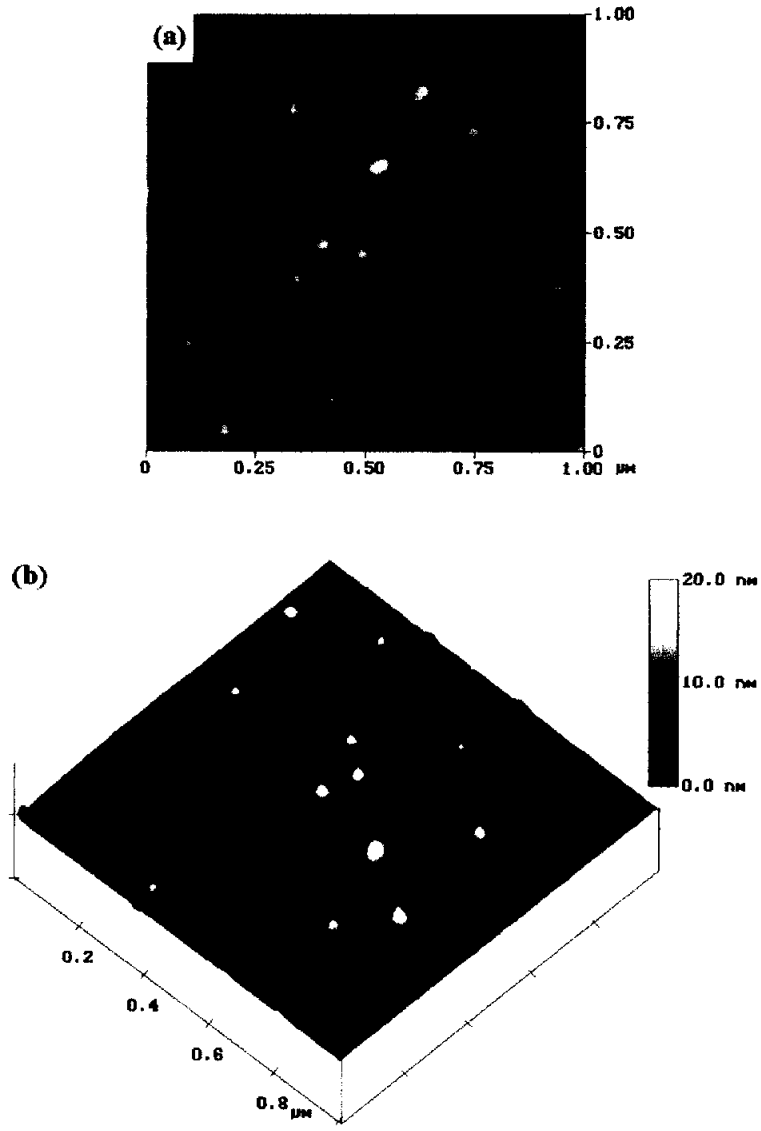

Figure 22 Top view on the surface image (a) and three-dimensional surface morphology (b) of Langmuir-Blodgett film of CdS nanoparticle deposited onto mica surface at 15 mN/m surface pressure with two layers obtained with AFM.

3-3. Characterization of PVA/CdS and CdSe nanocomposites

3-3-1. UV-vis absorption spectra

We made PVA nanocomposite using the synthesized CdS or CdSe nanoparticles by easy and simple method. In Figure 21, UV-vis absorption peak of PVA nanocomposite is consistent with that of the synthesized CdS or CdSe nanoparticles. In case of only PVA resin, it has not special absorption peak. These data revealed successful synthesis of PVA nanocomposite using nanoparticles.

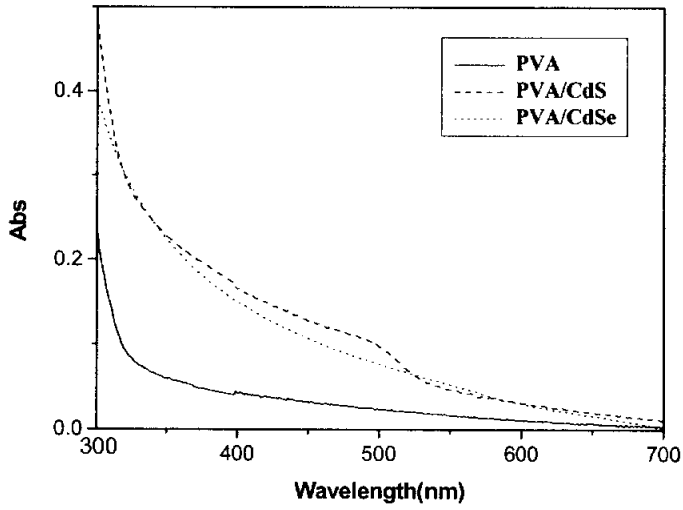

Figure 23 UV-vis absorption spectra of PVA/CdS and PVA/CdSe nanocomposites.

Polymer	Maximum absorbance wavelength (nm)
Polyester	352
Polystyrene	318
Polyethylene	300
Polypropylene	310
Polyvinyl chloride	310
Polycarbonate	235

Table 2 UV-vis absorption wavelength (λ_{max}) of various polymer materials.

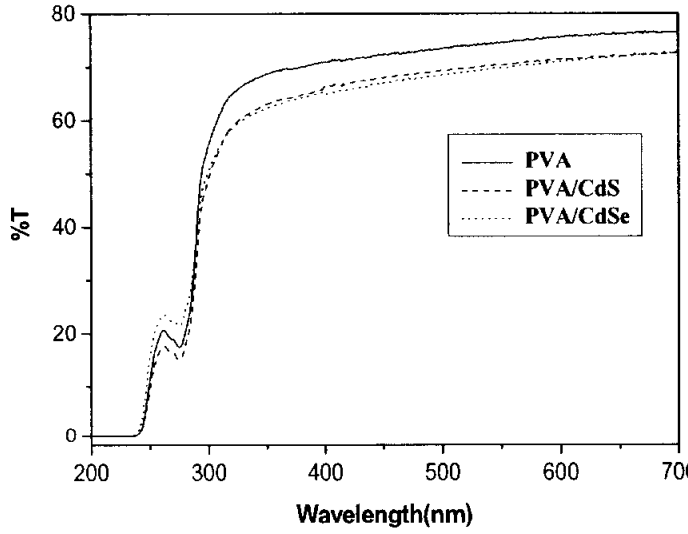

Figure 24 UV-vis transmission spectra of PVA/CdS and PVA/CdSe nanocomposites.

3-3-2. UV-vis transmission spectra

The obtained spectra of UV-vis transmission show dispersion degree of nanoparticles into PVA resin. In this case, the synthesized CdS or CdSe nanoparticles were well dispersed in PVA resin. If CdS or CdSe nanoparticles were not uniformly dispersed, transmittance of UV- vis wavelength will be decreased by irregular dispersion of nanoparticles. These spectra of PVA/CdS or CdSe nanocomposite were similar to that of PVA resin having no nanoparticles.

3-3-3. Photoluminescence (PL) study

Figure 23 shows the PL spectra of PVA nanocomposites containing CdS and CdSe nanoparticles according to different concentrations. The PL spectra are consistent with those of the synthesized CdS and CdSe nanoparticles. The PL intensity was increased with concentration of the added nanoparticles. But the PL intensity was not proportional to the exact amount of added CdS and CdSe. This is due to the sintering effect of emitted light by the neighboring nanoparticles in the polymer matrices. This is also partly because the added CdS or CdSe nanoparticles were not evenly dispersed in PVA nanocomposite. These PVA nanocomposites absorb the ultraviolet region wavelength light (< 400 nm) and emit the visible wavelength light.

The polymeric resins such as PVA or LDPE are subject to attack by UV light because of the organic nature of the polymer. UV lights are readily absorbed by certain organic functional group and excited to a higher energy state and then free radicals are formed, the

degradation process has begun. In the process, free radicals react with atmospheric oxygen to generate peroxy radicals. These very quickly form hydroperoxide which in turn generate a radical on the polymer backbone itself. The weak hydroperoxide will cleave easily in the presence of heat and sunlight and produce more radicals. Polymer absorbs UV light to generate a photoexcited state. Peroxyradical abstracts a hydrogen from adjacent molecules. As this process occurs, the polymers are slowly degraded and broken down. To suppress this process, the synthesized nanoparticles are doped into the polymeric resins. UV light can be converted into visible light by nanoparticles. The synthesized PVA or LDPE composite films absorb the ultraviolet region wavelength light (< 400 nm) and emit the visible wavelength light. Thus, these composite films have various advantages for the wavelength modification of light.

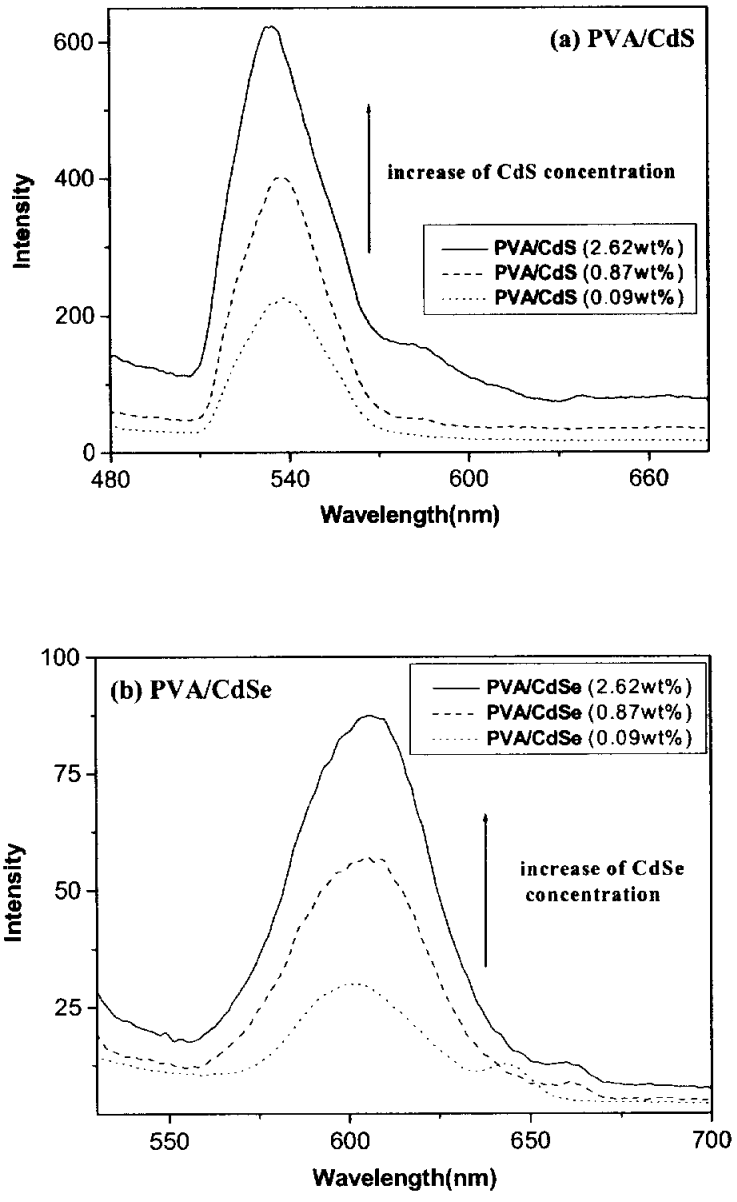

Figure 25 Photoluminescence spectra of (a) PVA/CdS, (b) PVA/CdSe nanocomposites according to concentration of CdS and CdSe nanoparticles, respectively.

3-3-4. Optical images

The synthesized PVA/CdS or CdSe nanocomposites were measured by optical microscopy to know degree of dispersion. The small black shapes had regard for the impurities of original PVA resin. Nanocomposites had yellow and brown color because of the added CdS and CdSe nanoparticles. In these images, we observed the good dispersion without aggregated nanoparticles.

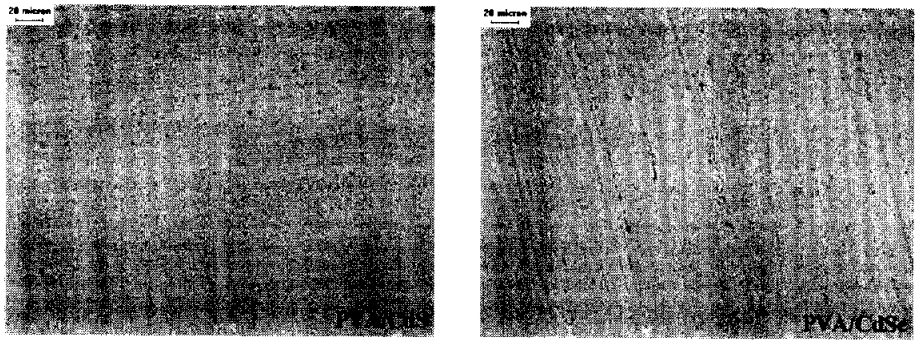

Figure 26 Optical images of PVA/CdS and PVA/CdSe nanocomposite.

3-4. Characterization of LDPE/CdS and CdSe nanocomposite

3-4-1. UV-vis absorption spectra

The properties of LDPE/CdS or CdSe nanocomposites were the same as those of PVA nanocomposites. UV-vis absorption spectra showed the same results of the synthesized CdS or CdSe nanoparticles. These data displayed the higher absorbance of UV wavelength (300 - 400 nm) than that of LDPE resin.

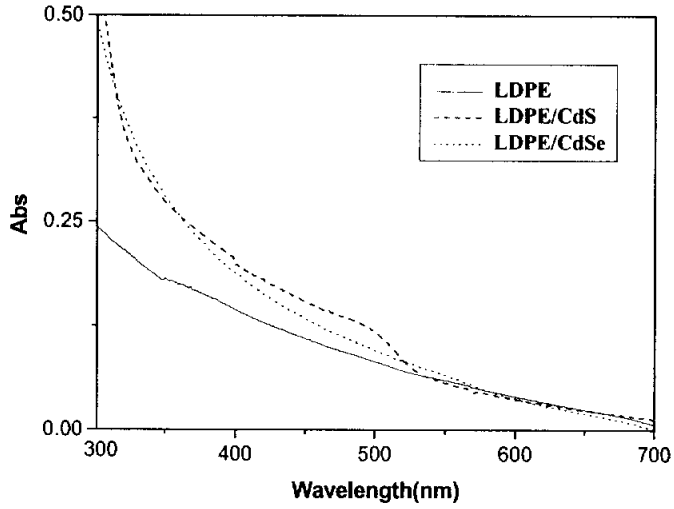

Figure 27 UV-vis absorption spectra of LDPE/CdS and LDPE/CdSe nanocomposites.

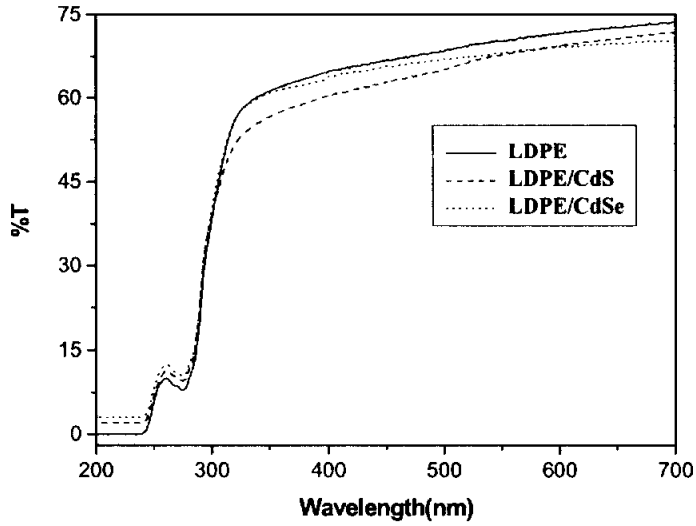

Figure 28 UV-vis transmission spectra of LDPE/CdS and LDPE/CdSe nanocomposites.

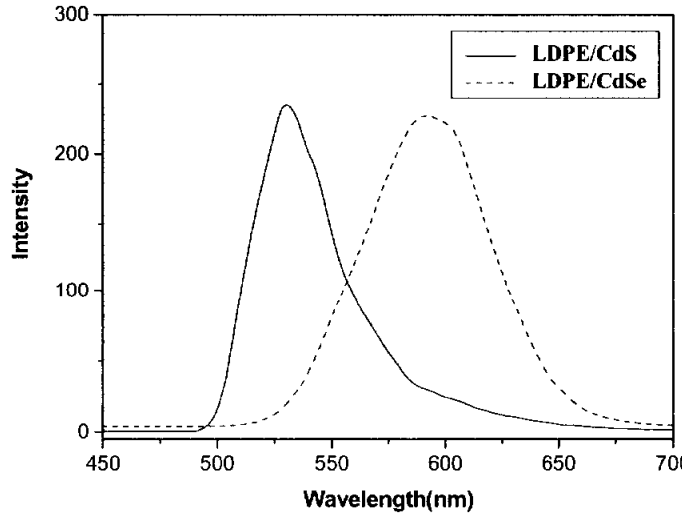

Figure 29 Photoluminescence spectra of LDPE/CdS and LDPE/CdSe nanocomposites.

3-4-2. UV-vis transmission spectra

UV-vis transmission spectra exhibited dispersion property of the added nanoparticles into LDPE resin. Transmittance is about 75% at 700 nm and sharply decreases at 320 nm. There is little difference between LDPE/CdS or CdSe nanocomposites and LDPE resin only. Thus, LDPE nanocomposites were successfully synthesized and have good dispersion.

3-4-3. Photoluminescence (PL) study

The PL spectra of LDPE/CdS or CdSe nanocomposites are consistent with those of the synthesized CdS and CdSe nanoparticles. LDPE nanocomposites absorb UV light by the added CdS or CdSe nanoparticles and then emit visible light of 520 and 600 nm, respectively.

3-4-4. Optical images

The optical image of LDPE/CdS nanocomposites showed evenly dispersed CdS nanoparticles. LDPE/CdSe nanocomposites have a few aggregated particles. These images displayed good dispersion in large part.

3-4-4. Scanning electron microscopy (SEM)

The SEM sample was prepared by cutting off a middle part of LDPE/CdS nanocomposites. SEM image indicated dispersion property such as previous optical images. The used LDPE nanocomposites has not aggregation of the mixed CdS nanoparticles. It shows dispersion degree of the inside of LDPE nanocomposites.

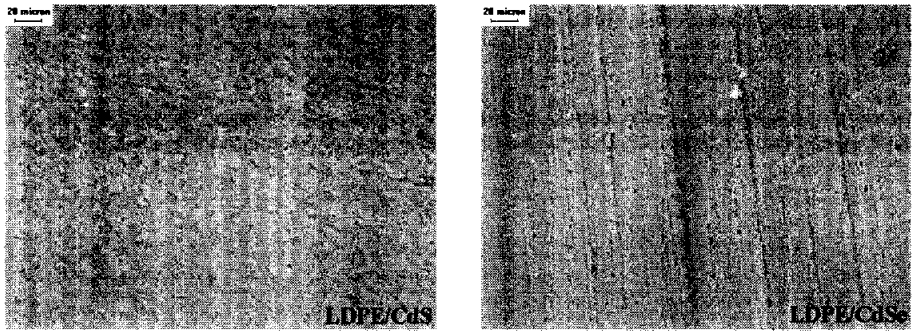

Figure 30 Optical images of LDPE/CdS and LDPE/CdSe nanocomposites.

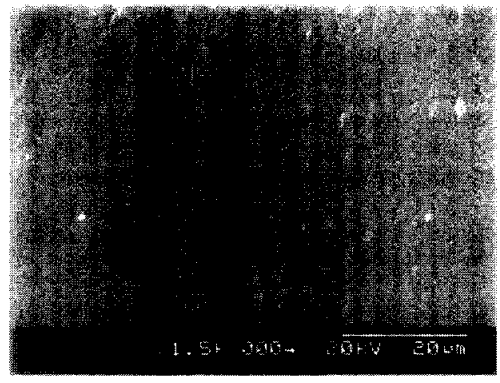

Figure 31 Scanning electron microscopy (SEM) image of the section of LDPE/CdS nanocomposite.

4. Conclusion

Semiconducting nanoparticles of CdS and CdSe were synthesized by thermal treatment using sodium oleate as capping surfactant and PVA or LDPE composite films containing the synthesized nanoparticles. From TEM images, the particle size of these nanoparticles was determined as 2 - 13 nm. Photoluminescence spectra of CdS and CdSe nanoparticles showed emission wavelength (λ_{max}) at 520 nm and 600 nm, when excited at 365 nm, respectively. That is, these nanoparticles absorb the UV light (200 ~ 400 nm) and emit visible light (400 - 700 nm). The synthesized nanoparticles show strong band-edge of photoluminescence. PL of the synthesized nanoparticles showed wavelength modification into visible region when excited at UV wavelength. For the structural characterization, sodium oleate was successfully used to replace the surfactant molecules on surface of nanoparticles. CdS and CdSe nanoparticles will be used as light wavelength modification materials by doping greenhouse films for the utilization of plant growth acceleration. PVA and LDPE nanocomposite containing CdS and CdSe nanoparticles were successfully synthesized. UV-vis and PL spectra of nanocomposite were consistent with those of the synthesized nanoparticles. The synthetic procedures developed in the present study offer several important advantageous features for the synthesis of nanoparticles. The synthetic process is very easy and inexpensive. Also, the synthetic method is a generalized process that can be applied to synthesize different kinds of semiconducting nanoparticles. The dispersion and stability in the PVA and LDPE were also studied and determined as excellent.

5. References

1. Klabunde, K. J. Nanoscale Materials in Chemistry, Wiley-InterScience: New York, (2001).
2. Arnim, H. *Chem. Rev.*, **1998**, *89*, 1861.
3. Arders, H.; Michael, G. *Chem. Rev.*, **1995**, *95*, 49.
4. Hu, J.; Li, L. S.; Yang, W.; Manna, L.; Wang, L. W.; Alivisators, A. P. *Science*, **2001**, *292*, 2060.
5. Weller, H. *Adv. Mater.* **1993**, *5*, 88.
6. Beecroft, L. L.; Ober, C. K. *Chem. Mater.* **1997**, *9*, 1302.
7. Encai, H.; Haiping, S.; Junqiu, L.; Bai, Y.; Jiacong, S. *Chem. Mater.* **1999**, *11*, 3096.
8. Wang, Y.; Herron, N.; *J. Phys. Chem.* **1991**, *95*, 526.
9. Pileni, M. P. *J. Phys. Chem.* **1993**, 97, 6961.; Pileni, M. P. *Langmuir.* **1997**, *13*, 3266.
10. Korgel, B. A.; Monbouquette, H. G. *J. Phys. Chem.* **1996**, *100*, 346.
11. Spanhel, L.; Hasse, M.; Weller, H.; Henglein, A. *J. Am. Chem. Soc.* **1987**, *109*, 5649.
12. Vossmeyer, T.; Katsikas, L.; Giersig, M.; Popovic, I. G.; Diesner, K.; Chemseddine, A.; Eychmuller, A.; Weller, H. *J. Phys. Chem.* **1994**, *98*, 7665.
13. Rockenberger, J.; Troger, L.; Kornowski, A.; Vossmeyer, T.; Eychmuller, A.; Feldhaus, J.; Weller, W. *J. Phys. Chem. B* **1997**, *101*, 2691.

14. Murray, C. B.; Norris, D. J.; Bawendi, M. G. *J. Am. Chem. Soc.* **1993**, *115*, 8706.
15. Diaz, D.; Rivera, M.; Ni, T.; Rodriguez, J. C.; Castillo-Blum, S. E.; Nagesha, D.; Robles, J.; Alvarez-Fregoso, O. J.; Kotov, N. A. *J. Phys. Chem. B* **1999**, *103*, 9854.
16. Nirami, M.; Murray, C. B.; Bawendi, M. G. Phys. Rev. B **1994**, *50*, 2293.
17. Huang, J.; Yang, Y.; Yang, B.; Liu, S.; Shen, *J. Polym. Bull.* **1996**, *36*, 337.
18. Stucky, G. D.; MacDougall, J. E. *Science* **1990**, *247*, 669.
19. Yang, P.; Zhao, D.; Margolese, D. I.; Chmelka, B. F.; Stucky, G. D. *Nature* **1998**, *396*, 152.
20. Hirai, T.; Okubo, H.; Kamasawa, I. *J. Phys. Chem. B* **1999**, *103*, 4228.
21. Weller, H. *Angew. Chem., Int. Ed. Engl.* **1993**, *32*, 41.
22. Facsko, S.; Dekorsy, T.; Koerdt, C.; Trappe, C.; Kurz, H.; Vogt, A.; Hartnagel, H. L. *Science* **1999**, *285*, 1551.
23. Pileni, M. P. *Langmuir* **1997**, *13*, 3266.
24. Lin, X. M.; Sorensen, C. M.; Klabunde, K. J.; Hajipanayis, G. C. *L. Mater. Res.* **1999**, *14*, 1542.
25. Sugimoto, T.; Chen, S.; Muramatsu, A. *Colloids Surf. A* **1997**, *135*, 207.
26. Trindade, T.; O Brien, P.; Zhang, X.-m. *Chem. Mater.* **1997**, *9*, 523.
27. Trindade, T.; O Brien, P. *J. Mater. Chem.* **1996**, *6*, 343.
28. Martin, C. R. *Science* **1994**, *266*, 1961.

29. Zhao, X. K.; Herve, P. J.; Fendler, J. H. *J. Phys. Chem.* **1989**, *93*, 208.
30. Meldrum, F. C.; Kotov, N. A.; Fendler, J. H. *Chem. Mater.* **1995**, *7*, 1112.
31. Moffit, M.; Eisenberg, A. *Chem. Mater.* **1995**, *7*, 1178.
32. Moffit, M.; Mcmahon, L.; Pessel, V.; Eisenberg, A. *Chem. Mater.* **1995**, *7*, 1185.
33. Gorer, S.; Albu-Yaron, A.; Hodes, G. *Chem. Mater.* **1995**, *7*, 1243.
34. Charych, D. H.; Majda, M. *Thin Solid Films* **1992**, *210/211*, 348.
35. Du, Z.; Zhang, Z.; Zhao, W.; Zhu, Z.; Zhang, J.; Jin, Z.; Li, T. *Thin Solid Films* **1992**, *210/211*, 404.
36. Lane, N. *Journal of Nanoparticle Research* **2001**, *3*, 95.
37. Service, R. F. *Science* **2000**, *290*, 1526.
38. Atkins, P. W. *Physical Chemistry*; 3 ed.; Oxford University Press: Oxford, **1986**.
39. Karplus, M.; Porter, R. N. *Atoms and Molecules*; 1 ed.; W. A. Benjamin, Inc.: NewYork, **1970**.
40. Alivisatos, A. P. *Endeavour* **1997**, *21*, 56.
41. Alivisatos, A. P. *Science* **1996**, *271*, 933.
42. Murray, C. B.; Norris, D. J.; Bawendi, M. G. *J. Am. Chem. Soc.* **1993**, *115*, 8706.
43. Peng, X.; Wickham, J.; Alivisatos, A. P. *Journal of the Ameriacan Chemical Society* **1998**, *120*, 5343.
44. Yang, J. P.; Meldrum, F. C.; Fendler, J. H. *J. Phys. Chem.* **1995**, *99*, 5500.

45. Yu, S. H.; Wu, Y. S.; Yang, J.; Han, Z. H.; Xie, Y.; Qian, Y. T.; Liu, X. M. *Chem. Mater.* **1998**, *10*, 2309.

46. (a) O Neil, M.; Marohn, J.; McLendon, G. *J. Phys. Chem.* **1990**, *94*, 4356. (b) O Neil, M.; Marohn, J.; McLendon, G. Chem. *Phys. Lett.* **1990**, *168*, 208.

47. Misawa, K.; Yao, H.; Hayashi, T.; Kobayashi, T. Chem. *Phys. Lett.* **1991**, *183*, 113.

48. Hasselbarth, A.; Eychmuller, A.; Weller, H. *Chem. Phys. Lett.* **1993**, *203*, 271.

49. (a) Rossetti, R.; Brus, L. E. *J. Phys. Chem.* **1986**, *90*, 558. (b) Chestnoy, N.; Harris, T. D.; Hull, R.; Brus, L. E. *J. Phys. Chem.* **1986**, *90*, 3393.

50. (a) Klimov, V.; Haring Bolivar, P.; Kurz, H. *Phys. ReV. B.* **1996**, *53*, 1463. (b) Klimov, V. I.; Haring-Bolivar, P.; Kurz, H.; Karavinskii, V. A. *Superlattices Microstruct.* **1996**, *20*, 395. (c) Hursche, S.; Dekorsy, T.; Klimov, V.; Kurz, H. *Appl. Phys. B.* **1996**, *62*, 3.

51. Arai, T.; Orii, T.; Ichikawa, H.; Onari, S.; Matsuishi, K. *Mater. Sci. Eng. A* **1996**, *217*, 159.

52. Garuthara, R.; Levine, G. *J. Appl. Phys.* **1996**, *80*, 401.

53. Jaeckel, G. *Z. Tech. Phys.* **1926**, *6*, 301.

54. Brus, L. E. *J. Chem. Phys.* **1984**, *80*, 4403.

55. Gaponenko, S. V. *Optical Properties of Semiconductor Nanocrystals*; Cambridge

56. Bawendi, M. G.; Steigerwald, M. L.; Brus, L. E. *Annu. Rev. Phys. Chem.* **1990**, *41*, 477.

57. Murray, C. B.; Norris, D. J.; Bawendi, M. G. *J. Am. Chem. Soc.* **1993**, *115*, 8706.

58. Klimov, V. I.; McBranch, D. W.; Leatherdale, C. A.; Bawendi, M. G. *Phys. Rev. BCondens Matter* **1999**, *60*, 13740.

6. Korean Abstract

CdS와 CdSe 나노입자는 복합체 계면활성제로 sodium oleate를 사용하여 열처리를 이용한 방법으로 성공적으로 합성되었다. Sodium oleate는 고온、고압법에 의한 CdS와 CdSe 나노입자를 합성하는 데 효과적인 계면활성제를 이용되어졌다. CdS와 CdSe 무기 나노입자와 같은 물질은 발광현상을 나타낸다. 입자크기가 2.6 - 13 nm인 CdS와 CdSe 나노입자는 365 nm의 파장에서 여기 되었을 때 각각 520 nm와 600 nm의 발광파장을 나타낸다. 합성된 나노입자의 발광현상은 자외선의 빛으로 여기 되었을 때, 가시광 영역의 파장으로 광파장 전환되는 것을 보여준다. PVA와 LDPE 수지에 도핑된 나노입자들은 유기/무기 나노컴퍼지트 (PVA/CdS, CdSe 또는 LDPE/CdS, CdSe)를 형성한다. PVA와 LDPE 같은 필름수명은 자외선 조사에 의한 polyolefin 필름에서의 C=O와 C=C 이중결합의 분해로 인해 감소하게 된다. 결과적으로, 필름의 물리적 특성은 변하게 된다. 이러한 현상은 필름에 손상을 입히는 자외선 빛을 흡수하는 파장 전환 나노입자를 필름에 도핑함으로써 억제된다. 합성된 나노입자와 나노컴퍼지트의 특성은 흡수, 투과, 발광, XRD, TEM, SEM 등의 측정으로 알 수 있었다.